ISSN 1819-7140, Russian Journal of Pacific Geology, 2011, Vol. 5, No. 4, pp. 313–335. © Pleiades Publishing, Ltd., 2011.
Original Russian Text © S.V. Zyabrev, 2011, published in Tikhookeanskaya Geologiya, 2011, Vol. 30, No.4, pp. 49–73.

Stratigraphy and Structure of the Central East Sakhalin Accretionary Wedge (Eastern Russia)

S. V. Zyabrev

Kosygin Institute of Tectonics and Geophysics, Far East Branch, Russian Academy of Sciences, ul. Kim Yu Chena 65, Khabarovsk, 680000 Russia

e-mail: sziabrev@ itig.as.khb.ru

Received November 18, 2010

Abstract—The East Sakhalin accretionary wedge is a part of the Cretaceous–Paleogene accretionary system, which developed on the eastern Asian margin in response to subduction of the Pacific oceanic plates. Its formation was related to the evolution of the Early Cretaceous Kem–Samarga island volcanic arc and Late Cretaceous–Paleogene East Sikhote Alin continental-margin volcanic belt. The structure, litho-, and biostratigraphy of the accretionary wedge were investigated in the central part of the East Sakhalin Mountains along two profiles approximately 40 km long crossing the Nabil and Rymnik zones. The general structure of the examined part of the accretionary wedge represents a system of numerous east-vergent tectonic slices. These tectonic slices. tens to hundreds of meters thick. are composed of various siliciclastic rocks, which were formed at the convergent plate boundary, and subordinate oceanic pelagic cherts and basalts, and hemipelagic siliceous and tuffaceous–siliceous mudstones. The siliciclastic deposits include trench-fill mudstones and turbidites and draping sediments. The structure of the accretionary wedge was presumably formed owing to off-scraping and tectonic underplating. The off-scraped and tectonically underplated fragments were probably tectonically juxtaposed along out-of-sequence thrusts with draping deposits. The radiolarian fauna was used to constrain the ages of rocks and time of the accretion episodes in different parts of the accretionary wedge. The defined radiolarian assemblages were correlated with the radiolarian scale for the Tethyan region using the method of unitary associations. In the Nabil zone, the age of pelagic sediments is estimated to have lasted from the Late Jurassic to Early Cretaceous (Barremian); that of hemipelagic sediments, from the early Aptian to middle Albian; and trench-fill and draping deposits of the accretionary complex date back to the middle–late Albian. In the Rymnik zone, the respective ages of cherts, hemipelagic sediments, and trench facies with draping deposits have been determined as Late Jurassic to Early Cretaceous (middle Albian), middle Aptian–middle Cenomanian, and middle–late Cenomanian. East of the rear toward the frontal parts of the accretionary wedge, stratigraphic boundaries between sediments of different lithology become successively younger. Timing of accretion episodes is based on the age of trench-fill and draping sediments of the accretionary wedge. The accretion occurred in a period lasting from the terminal Aptian to the middle Albian in the western part of the Nabil zone and in the middle Cenomanian in the eastern part of the Rymnik zone. The western part of the Nabil zone accreted synchronously with the Kiselevka–Manoma accretionary wedge located westerward on the continent. These accretionary wedges presumably formed along a single convergent plate margin, with the Sakhalin accretionary system located to the south of the Kiselevka–Manoma terrane in the Albian.

Keywords: *structure, stratigraphy, radiolarians, Mesozoic, accretionary tectonics, Sakhalin, eastern Russia.*

DOI: 10.1134/S1819714011040087

INTRODUCTION

The East Sakhalin accretionary wedge is a part of the Cretaceous–Paleogene accretionary system, which developed in eastern Asia first as an island arc and then as a continental-margin structure in response to subduction of the oceanic plates of the Northwest Pacific [9, 22, 30, 36, 37, 62]. This accretionary system also includes the Early Cretaceous–Cenozoic West Sakhalin forearc trough, Early Cretaceous island arc (its Moneron–Rebun–Kabato and Kem–Samarga fragments), and Late Cretaceous–Paleogene East Sikhote Alin continental-margin volcanic belt (Fig. 1). Terrigenous sedimentation in the West Sakhalin trough started in the Aptian [14]. The island arc formed in the Aptian–Albian [6, 20, 31, 33], and the volcanic belt was initiated in the Cenomanian [23, 32].

The accretionary wedge represents a scaly–thrust structure composed of intensely deformed volcanogenic–siliceous, terrigenous, and metamorphic rocks with ophiolitic massifs [9, 22, 24, 25, 28, 36, 37]. The age of the accretionary wedge remains debatable. For example, Parfenov [22] believes that its western and eastern parts developed in response to the evolution of

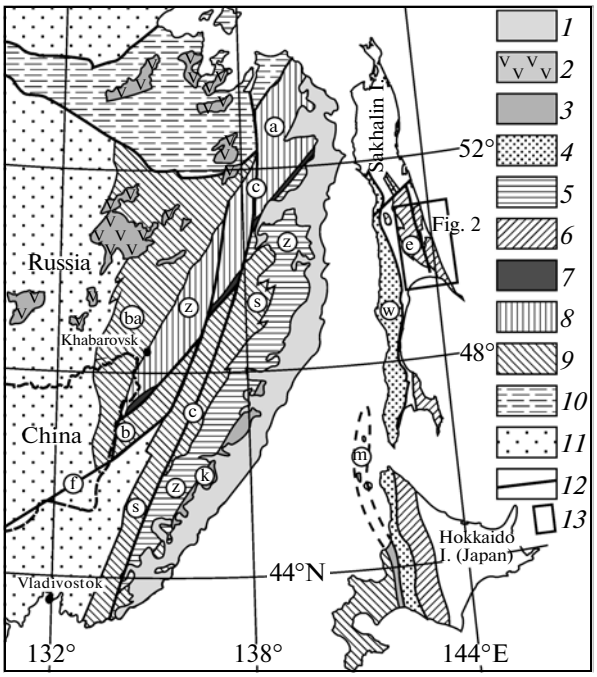

Fig. 1. Schematic tectonic map of the Russian Far East and adjacent regions, modified after [21, 48, 56], and position of the studied area.

(*1*) Late Cretaceous–Paleocene East Sikhote Alin volcanic belt (esa); (*2*) Early–Late Cretaceous Khingan–Okhotsk volcanic belt; (*3*) fragments of the Early Cretaceous volcanic arc: (k) Kem–Samarga, (m) Moneron–Rebun–Kabato; (*4*) forearc trough of West Sakhalin (w) and Hokkaido (Aptian–Cenozoic); (*5*) Early Cretaceous turbidite trough, Zhuravlevka terrane (z); (*6–9*) accretionary wedges: (*6*) Cretaceous, East Sakhalin (e) and Hokkaido, (*7*) Aptian–Albian, Kiselevka–Manoma terrane, (*8*) Early Cretaceous, Amur terrane (a), (*9*) Jurassic–Early Cretaceous, Badzhal (ba), Bikin (b), and Samarka (s) terranes; (*10*) Mongol–Okhotsk suture zone; (*11*) cratonic domains; (*12*) major faults: (c) Central Sikhote Alin, (f) Fushun–Mishan; (*13*) studied area.

the Late Mesozoic island arc and Late Cretaceous–Paleogene active continental margin, respectively. Khanchuk [36, 37] argues that the western part of the accretionary wedge (Aniva–Gomon terrane) formed in the Early–Late Cretaceous (Albian–Cenomanian), and its eastern segment (Nabil terrane), in the Late Cretaceous (Late Cretaceous–Paleocene).

With the present-day state of stratigraphic knowledge about the accretionary wedge, it is impossible to construct detailed evolutionary models of it. The available stratigraphic concepts are largely based on materials obtained by geological mapping in the second half of the 20th century [5]. The defined stratigraphic units (formations united into groups) are characterized by significant thicknesses and reiteration of volcanogenic–siliceous and siliciclastic members in their sections [5], which is inconsistent with present-day views on the stratigraphy and evolution of accretionary wedges. The type stratigraphic succession of accreted strata begins with oceanic pelagic sediments that are subsequently replaced higher in the section by hemipelagic and terrigenous facies of the deep trench [54, 55]. Such a succession reflects the history of sedimentation on the oceanic plate that was moving from the spreading center toward the subduction zone to be incorporated there into the accretionary wedge [46, 54, 55].

A biostratigraphic investigation in some areas of East Sakhalin revealed the development of similar rock successions [1, 27, 28], which provided evidence for formation timing of isolated fragments of the accretionary wedge. Nevertheless, the available stratigraphic data are insufficient for reconstructing a more complete evolutionary model of it. The application of radiolarians for age determination changed the stratigraphic scheme of the accretionary wedge. By now, the most progress in stratigraphic revision was attained for the southern part of the accretionary wedge. Additional biostratigraphic and geological studies carried out in the Tonin–Aniva Peninsula not only made it possible to specify the age of facies-variable lithological units, but also to fundamentally change the stratigraphic model [12, 13]. The newly defined stratigraphic units lack reiteration of volcanogenic–siliceous and siliciclastic members, which are now distinctly subdivided by age. A new stratigraphy served as the basis for developing a detailed evolutionary model for this part of the accretionary wedge [11, 12].

Northward, in the East Sakhalin Mountains, the stratigraphic scheme remains practically unchanged. New finds of radiolarians were used just to revise the ages of previously defined stratigraphic units in their former lithostratigraphic succession. It is clear that new studies are needed to further develop the evolutionary model for the accretionary wedge. This work is dedicated to studying the general structure, litho-, and biostratigraphy of the accretionary wedge in the central part of the East Sakhalin Mountains. New radiolarian ages in facies-variable members make it possible to refine the stratigraphy and determine the age of accretion of different accretionary wedge fragments.

TECTONIC POSITION OF THE STUDY AREA

The examined part of the accretionary wedge is located in the central part of the East Sakhalin Mountains (Fig. 2) and includes the eastern part of the Aniva–Gomon zone, Pilenga–Nabil, and Rymnik subzones of the East Sakhalin zone [28], which approximately corresponds to the eastern part of the Aniva–Gomon terrane and Nabil terrane defined by A.I. Khanchuk [36, 37]. In the schematic tectonic map compiled by V.M. Grannik, the study area corresponds to the Gomon and Rymnik terranes [9]. Inasmuch as the exact position of boundaries for these lithotectonic zones/terranes in the above-mentioned small-scale schematic tectonic maps is ambiguous, the examined part of the accretionary wedge is subdivided

into the Nabil and Rymnik zones (Fig. 2), according to the distribution of the Nabil and Rymnik groups within their contours [4, 15, 18], which are separated from each other by the Pribrezhnyi meridional fault.

Areas located east of the Rymnik zone are occupied by Upper Cretaceous volcanic and volcanogenic–sedimentary rocks [4, 5, 7, 8] that were attributed to the Terpeniya subzone of the East Sakhalin zone in [28] and to the Terpeniya terrane, representing a fragment of the Late Cretaceous island arc in [8, 9, 36, 37]. Metamorphic rocks of the accretionary wedge distributed west of the Nabil zone are either referred to the Aniva–Gomon zone [28] or are defined as the Val'zin terrane [9].

EVOLUTION OF VIEWS ON STRATIGRAPHY AND AGE OF ROCKS

In the examined area of the **Nabil zone,** volcanogenic–siliceous and siliciclastic rocks are attributed to the Ostraya and Khoi formations that are united into the Nabil Group [4, 5, 18]. The Ostraya Formation (1500–2000 m) is characterized by the heterogeneous composition (shales, siltstones, and sandstones with several volcanogenic–siliceous units of jaspers, siliceous–clayey shales, limestones, and spilites) and significant facies variability along the strike [5]. The overlying Khoi Formation (2200 m) is relatively uniform in lithology being largely composed of sandstones, shales, and siltstones with subordinate siliceous–clayey shales, jaspers, limestones, and volcanics [5]. The relatively conditional Jurassic–Cretaceous age of both formations is inferred from finds of hexacorals, gastropods, and foraminifers in limestones [5]. The radiolarian assemblage from cherts (Nabil assemblage) was determined as undoubtedly Mesozoic, most likely, Jurassic in age [5, 10]. Subsequently, Rozhdestvenskii [29] included two additional units into the Nabil Group: Pravyi Nabil siliceous–volcanogenic (600–2500 m) and Lopatin terrigenous, substantially sandy (>2200 m) formations. This author considered the age of these sequences overlying the Khoi Formation to be Late Jurassic–Early Cretaceous and Albian–Cenomanian, respectively.

The age of the Nabil Group was substantially revised after lithologic–stratigraphic investigations by A.N. Rechkin and I.Yu. Zharov in 1982–1985. A thorough study of sections was accompanied by dating of numerous samples by radiolarians, which were studied by L.I. Kazintsova. Owing to these studies, the Ostraya and Khoi formations were dated back to the Albian–Cenomanian and Cenomanian, respectively. Moreover, the thick (2900 m) Ivashka olistostrome of Cenomanian–Turonian age was defined within the Khoi Formation. Kazintsova gave a description of radiolarian assemblages and determined the respective ages of the Ostraya and Khoi formations as being late Albian–Cenomanian and late Cenomanian–early Turonian, respectively [16].

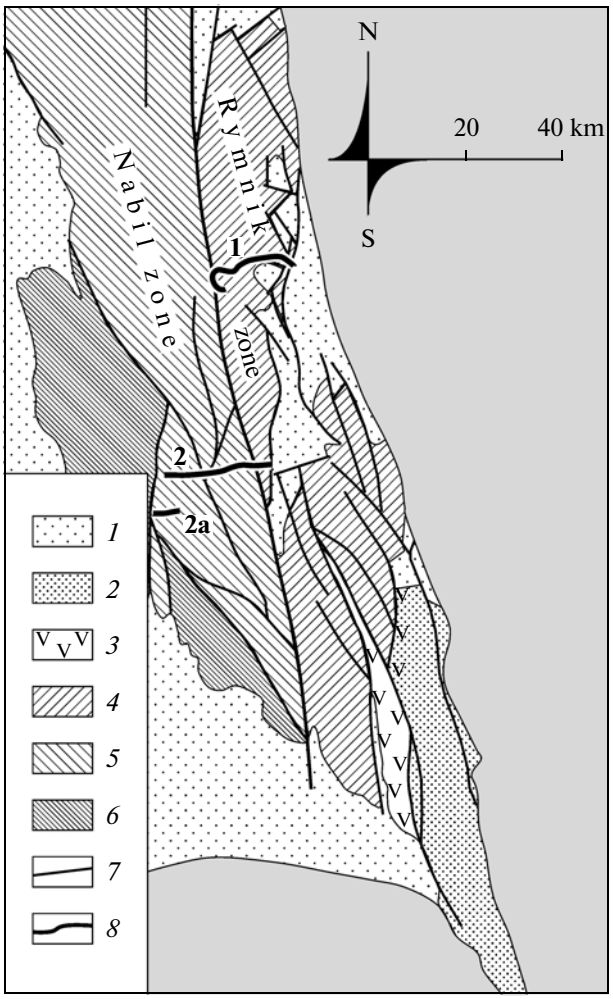

Fig. 2. Schematic tectonic map of the studied area (after [4, 18]) and position of routes.

(*1*) Cenozoic sediments of the Tym–Poronai depression and grabens; (*2*) Upper cretaceous volcanogenic–sedimentary deposits; (*3*) Upper Cretaceous island-arc volcanics; (*4–6*) accretionary wedge: (*4*) Rymnik zone, (*5*) Nabil zone, (*6*) metamorphic complex; (*7*) faults; (*8*) routes: (**1**) Langeri River, (**2**) Sprut–Pilenga rivers, (**2a**) isolated outcrops along the Ivashka River.

In the western areas of East Sakhalin, Rikhter and Bragin established transition from siliceous to terrigenous sedimentation in the Albian–Cenomanian [27, 28]. These researchers found Valanginian–Barremian radiolarians in cherts and their Albian–Cenomanian assemblages in siliceous mudstones and terrigenous siltstones of the Nabil Group outcropping in the Pilenga and Ivashka river basins [1, 28]. Recently, Vishnevskaya described and illustrated the Valanginian, Barremian, and Aptian–early Albian radiolarian assemblages from the volcanogenic–siliceous rocks of the Nabil Group [2, 3].

In the **Rymnik zone**, volcanogenic–siliceous and terrigenous rocks are attributed to the Bogataya, Rakita, and Berezovsk formations of the Rymnik Group

[5, 7]. The Bogataya Formation, 1200–1600 m thick, is made up of siliceous mudstones and siltstones with subordinate tuffs and tuffites. The Rakita Formation, 1300–1400 m thick, is characterized by a composition similar to the previous unit, differing from the latter in a significant content of jaspers, basalts, and limestones. The Berezovsk Formation, 3000–4000 m thick, unites the siliciclastic, calcareous–siliceous, and volcanogenic rocks. Raznitsyn considers that the Berezovsk Formation represents olistostrome with inclusions of siliceous–volcanogenic rocks of the Bogataya and Rakita formations and assumes wide development of olistostromes in East Sakhalin [24, 25].

Based on finds of large poorly preserved presumably radial–ridge inoceram shells, the Bogataya and Rakita formations were conditionally determined to be the Santonian–early Campanian and early Campanian in age, respectively; the Berezovsk Formation yielded late Campanian fauna of ammonites, inoceramas, and patellas [5]. Subsequently, based on additional paleontological finds, the ages of these units were determined as the Coniacian (?–early Santonian for the Bogataya Formation, the Santonian for the Rakita Formation, and late Santonian–Danian for the Berezovsk Formation [7]. It should be noted that most of the fossils were found in the eastern distribution band of the Rymnik Group near the sea coast. Based on radiolarians, Kazintsova determined the age of the Rakita Formation as the Campanian and, probably, Maastrichtian and that of the Berezovsk Formation, as the Maastrichtian and, probably, late Campanian [16].

As is evident from this review, the use of different fossil groups and their additional finds in facies-variable rocks have substantially transformed views on the age of stratigraphic units. The age estimates obtained for separate fragments of the sedimentary succession were frequently interpreted as reflecting the ages of whole stratigraphic units, which include facies-variable and heterochronous rocks distributed through the spacious region. Despite the long-existing interpretation of the East Sakhalin tectonic structure as an accretionary wedge, the preserved concept of volcanogenic–siliceous and terrigenous members alternating in the section reflects the geosynclinal approach. The age and stratigraphic range of siliceous, siliceous–clayey, and terrigenous rocks in different parts of the accretionary wedge remain unclear. The onset of terrigenous sedimentation, which is of particular significance for timing accretion episodes, is also undated. The incompleteness of available stratigraphic data requires additional litho- and biostratigraphic investigations combined with structural research.

OBJECTS, MATERIAL, AND METHODS

The structural, litho-, and biostratigraphic investigations of the Nabil and Rymnik zones of the accretionary complex were conducted along two latitudinal (each extended approximately 20 km) well-exposed geological sections across East Sakhalin (Fig. 2). The Nabil zone has been examined transversely in the Central Range: along the motor road on the right side of the Sprut River on the western slope and on its eastern slope in the upper reaches of the Pilenga River in outcrops along the river and parallel to the motor road. For the western part of the Nabil zone, additional biostratigraphic data were obtained from several isolated outcrops in the upper reaches of the Ivashka River 10 km south of its main intersection with the zone (Fig. 2). The Rymnik zone was studied in the extended outcrops along the Langeri River banks in its lower reaches.

The route geological maps compiled using geological, sedimentological, and structural observations (Figs. 3, 4) demonstrate different types of rocks, their attitude, and relations between each other. Radiolarians used for determining age of sediments and reconstructing stratigraphic successions were examined in many samples taken from siliceous, siliceous–clayey, and fine-detrital siliciclastic varieties.

ROCKS CONSTITUTING THE ACCRETIONARY WEDGE

The examined segment of the accretionary wedge is largely composed of siliciclastic rocks with volcanogenic–siliceous, siliceous–clayey, and carbonate varieties playing a subordinate role. Despite the established age differences, the rocks from the Nabil and Rymnik zones show significant lithological similarity and can be considered together.

Cherts (10–150 m) are represented by typical banded varieties with uniformly alternating thin beds of cherts (2–8 cm) and siliceous mudstones (up to

Fig. 3. Route geological map across the Nabil zone along the motor road in upper reaches of the Sprut and Pilenga rivers. The inset d shows epy position of routes a, b, and c.

(*1*) oceanic volcanogenic–siliceous and siliceous–clayey deposits; (*2*) trench-fill siltstones and turbidites; (*3*) draping sediments; (*4*) Cenozoic sediments (in graben); (*5*) faults; (*6*) isolated cherty and basaltic lenses; (*7*) basalts; (*8*) limestones; (*9*) cherts; (*10*) siliceous and tuffaceous–siliceous mudstones; (*11*) mudstones and siltstones; (*12*) thin- and thick-rhythmic turbidites; (*13*) thick- rhythmic turbidiies and turbidite sandstones; (*14*) chaotic sediments of debris flows; (*15*) tuffs and tuffaceous siltstones; (*16*) slumping deposits; (*17*) bedding attitude: normal (*a*), vertical (*b*), overturned (*c*); (*18*) cleavage attitude: normal (*a*) and vertical (*b*); (*19*) attitude of bedding and parallel cleavage: normal (*a*), vertical (*b*), overturned (*c*); (*20*) axes of synforms (*a*) and antiforms (*b*); (*21*) steep thrusts: proven (*a*) and hypothetical (*b*); (*22*) other faults: proven (*a*) and hypothetical (*b*); (*23*) position of samples with radiolarians with indication of their numbers and ages derived from radiolarian assemblages, including those according to the scale of unitary associations (lower row of numerals).

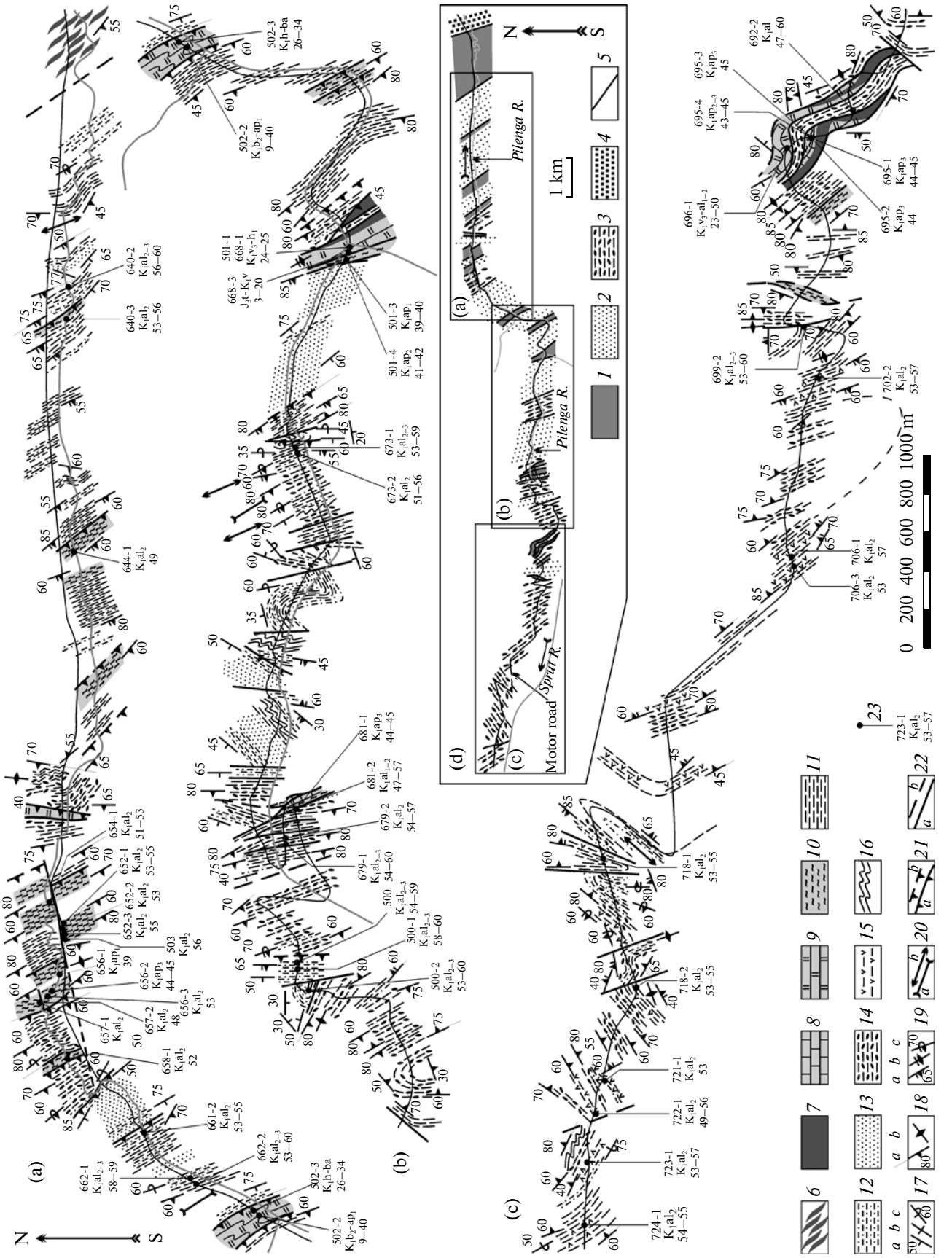
(a)
(b)
(c)
(d)
N
S
Pilenga R.
Spur R.
Motor road
1 km
0 200 400 600 800 1000 m

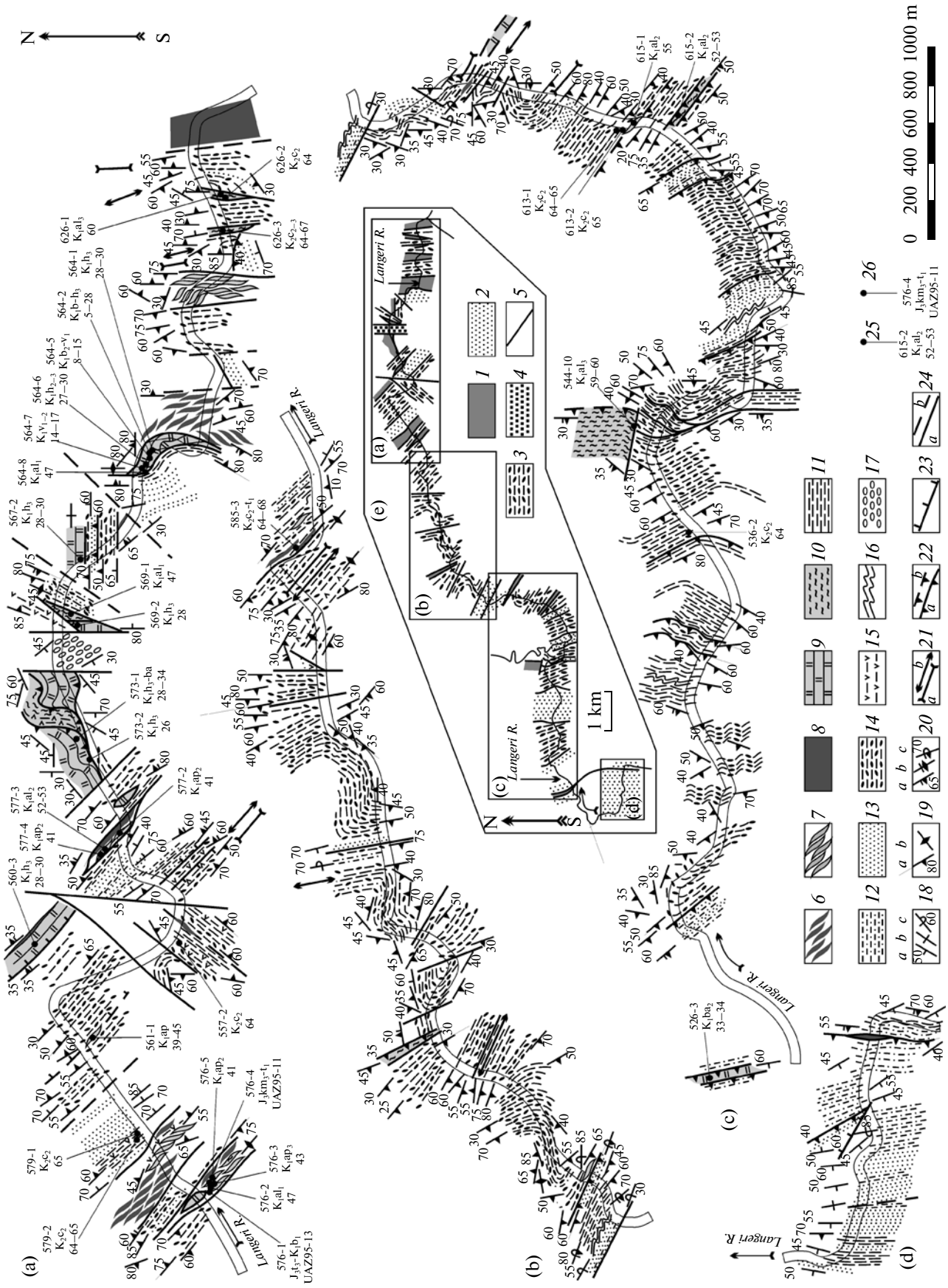
N
S
0 200 400 600 800 1000 m
1 km
Langeri R.
(a)
(b)
(c)
(d)
(e)

Fig. 4. The route geological map across the Rymnik zone in the lower reaches of the Langeri River. The inset E shows the position of routes a, b, c and d.

(*1*) oceanic volcanogenic–siliceous and siliceous–clayey deposits; (*2*) trench-fill siltstones and turbidites; (*3*) draping sediments; (*4*) Cenozoic sediments (in graben); (*5*) faults; (*6*) isolated cherty and basaltic lenses; (*7*) isolated cherty and siliceous mudstone lenses; (*8*) basalts; (*9*) cherts; (*10*) siliceous and tuffaceous–siliceous mudstones; (*11*) mudstones and siltstones; (*12*) thin- and medium- rhythmic turbidites; (*13*) thick-rhythmic turbidities and turbidite sandstones; (*14*) chaotic sediments of debris flows; (*15*) tuffs and tuffaceous siltstones; (*16*) slumping deposits; (*17*) Cenozoic sediments; (*18*) bedding attitude: normal (*a*), vertical (*b*), overturned (*c*); (*19*) cleavage attitude: normal (*a*) and vertical (*b*); (*20*) attitude of bedding and parallel cleavage: normal (*a*), vertical (*b*), overturned (*c*); (*21*) axes of synforms (*a*) and antiforms (*b*); (*22*) steep thrusts: proven (*a*) and hypothetical (*b*); (*23*) normal faults; (*24*) other faults: proven (*a*) and hypothetical (*b*); (*25*) position of samples with radiolarians with indication of their numbers and ages derived from radiolarian assemblages, including those according to the scale of unitary associations (lower row of numerals); (*26*) position of samples with radiolarians with indication of their numbers and ages derived from radiolarian assemblages, including those according to the scale of unitary associations (UAZ95) included (lower row).

1 cm). The cherts include coarse-bedded (from a few decimeters to a few meters thick) and more clayey varieties. They are mostly red, less commonly alternating with green and dark gray varieties. Radiolarian skeletons constitute from 30 to 70% of the rock volume. Some portions of the siliceous section contain beds (2–10 cm thick) of pinkish and gray micritic limestones. The cherts are locally crossed by a dense system of thin quartz veinlets and altered to microquartzites. Cherts represent typical pelagic sediments of the Mesozoic ocean [46, 54, 55].

Basalts (8–200 m) form a close spatial association with cherts. Despite their tectonic contacts, they frequently enclose cherty beds a few decimeters thick, which indicates their initial stratigraphic relations. Some basaltic flows are characterized by a pillow structure, while others are massive. Most of them show strong chloritization. Basalts are represented by tholeiitic and alkali varieties that were formed in spreading centers and hot spot settings [9, 37].

Micritic limestones (4–15 m) of light-gray coloration occur in two tectonic slices in the western part of the Nabil zone, where they are overlain by siliceous mudstones. In one of the slices, limestones rest upon basalts. It is assumed that limestones were formed at summits of underwater volcanic edifices. Massifs of reefal limestones a few kilometers in size known from the Nabil zone [19] were interpreted as representing fragments of paleoguyots [34, 35].

Siliceous and tuffaceous–siliceous mudstones (15–200 m), both massive and bedded are olive–gray or brown–red, or represented by decimetric alternation of variegated varieties. The rocks are to different extent saturated with dispersed pyroclastic material and frequently contain tuff and tuffaceous silicilith beds from several centimeters to several decimeters thick. Radiolarian skeletons are characterized by variable proportions, reaching 40 vol % in rocks with a minimal content of pyroclastic material. Siliceous mudstones represent typical hemipelagic sediments crowning sections of pelagic cherts in Mesozoic accretionary wedges [17, 54, 55]. In the examined part of the accretionary wedge, these rocks associate with cherts, but are always in tectonic contact.

Silicicalstic rocks form several characteristic sequences (tens to hundreds of meters thick) composed of genetically variable detrital varieties formed in different sedimentation settings.

Mudstones and siltstones (50–250 m) are characterized by thin bedding (2–8 cm) determined by variable admixtures of clayey material and the presence of sandy–silty laminae and their groups. Some mudstones are massive and intensely bioturbated. Members of mudstones and siltstones include rare thin turbidite (3–8 cm), tuffaceous siltstone, and silicified tuff (a few decimeters) beds. In the eastern part of the Nabil zone, the bedded mudstones and siltstones conformably overlie hemipelagic siliceous mudstones and higher in the section give way to thin- and medium-bedded turbidites (Fig. 3a). Mudstones and siltstones are interpreted as sediments formed by low-density turbidite and bottom (contour) currents in plain settings [40, 60, 72]. It is assumed that they accumulated in the frontal part of a deep-sea trench overlying hemipelagic sediments on the oceanic plate that reached the subduction zone.

Turbidites, which constitute a significant part of the accretionary wedge, are represented by their coarsely turbidites and turbiditic sandstones, which form thick (60–500 m) sedimentary successions. Beds up to 0.5–4.5 m thick are characterized by an erosional base and graded sorting of detrital material with distinct *abde* and *abcde* elements of the Bouma cycle [39]. The rhythm is largely composed of sandstones overlain by several centimeters of mudstones. Similarly thick beds of turbidite sandstones lack a mudstone roof and are characterized by a reduced set of *ab* and *a* sedimentary structures. Thick successions of coarse turbidites and turbidite sandstones are separated by intervals (4–15 m) of thin- to medium turbidites and silty pelites. Such turbidite successions are usually interpreted as sediments accumulated in sandy lobes and branching channels in the upper part of deep-sea fans [72]. Some turbidite successions (50–200 m thick) consist of thin- to medium turbidites (8–50 cm thick) with distinct parallel bed boundaries, erosional base, gradational sorting, and set of sedimentary *abcde, abde, bcde*, and *cde* elements of the Bouma cycle [39]. These turbidite successions either overlie mudstone parts of the sec-

tion or underlie thick-bedded turbidites and probably represent fragments of more complete turbidite series. Such sediments are deposited in more distal parts of deep-sea fans [72]. According to accepted interpretations, most of the turbidites constituting the accretionary wedge accumulated in the deep trench setting [55, 66, 71]. Thick-bedded turbidites are usually deposited in the axial part of the trench, while thin-bedded rhythms, in its frontal part [66]. Turbidites enclose tuff beds up to 2 m thick. In terms of lithology, turbidite sandstones are classed with graywackes; some of them are close to arkoses; all of them contain pyroclastic material [5, 26].

Chaotic sediments of debris flows are a typical component in the examined part of the accretionary wedge constituting together with associated stratified varieties approximately one-third of its volume. Beds of chaotic sediments of several meters to several tens of meters thick are composed of a uniform sandy–silty–clayey mass with irregularly distributed inclusions of variable compositions, morphologies, and sizes. The content of inclusions in the groundmass is highly variable, reaching 30%. The inclusions are represented by dominant sandstones and subordinate siliceous mudstones, tuffaceous siliciliths, cherts, microquartzites, basalts, and limestones. Their sizes vary from a centimeter to several meters across. There are both isometric and variably elongated inclusions; most of them are angular, although some of them are characterized by smoothed shapes. The inclusions of turbidite sandstones, tuffaceous siliciliths, and siliceous mudstones are frequently represented by deformed fragments of beds up to several decimeters thick and up to several meters long. The composition, proportion, and size of these inclusions are variable; basaltic and siliceous inclusions and larger fragments predominate near certain tectonic slices composed of these rocks. Many inclusions of basalts, cherts, siliceous mudstones, and tuffs demonstrate features reflecting tectonic impact on rocks prior to their burial in the groundmass such as cleavage, jointing, chloritization, and silicification.

Beds of chaotic deposits and their groups up to several tens of meters thick alternate in the section with bedded intervals of the comparable thickness. These intervals are largely composed of mudstones and siltstones with intercalations of tuffs, tuffaceous sittsones, and turbidites. Many mudstone and tuffaceous siltstone beds contain abundant radiolarian skeletons. Some separating intervals are composed of turbidites, including thick-bedded rhythmical members. Some bedded intervals demonstrate underwater slumping deformations. Successions of alternating chaotic and bedded deposits are several hundreds of meters thick.

The chaotic beds are made up of typical deposits of underwater debris flows that are generated on slopes [43, 44, 52]. Judging from lithology of the inclusions, these sediments were formed from destruction products of the accretionary wedge underlain by tectonically juxtaposed volcanogenic–siliceous and siliciclastic rocks. The accumulation area of debris flow and associated bedded sediments was probably limited by the slope of the accretionary wedge, since thicker successions of coarse turbidites in the axial part of the trench do not contain chaotic deposits. Similar alternation of chaotic deposits (of debris flows and slumping) with mudstones and turbidites was established by drilling in the sedimentary cover of basins that developed on slopes of present-day accretionary wedges in the Barbados Ridge area of the Caribbean Sea [63–65] and Nankai Trough in Japan [67–69]. By analogy with the recent setting, the alternating chaotic and stratified sediments of the area under consideration are interpreted as deposits draping the accretionary wedge.

STRUCTURE OF THE ACCRETIONARY WEDGE

The general structure of the examined part of the accretionary wedge represents a pile of many tectonic slices with different thicknesses, which are composed of oceanic volcanogenic–siliceous sediments, trench-fill deposits, and sediments draping the accretionary wedge slope (Figs. 3, 4). Different-facies sediments are usually separated by tectonic processes and only in several slices in the eastern part of the Nabil zone, hemipelagic siliceous mudstones are overlain by mudstones and trench-fill turbidites (Fig. 3a). The structure is characterized by the dominant N–NW strike of slices and their steep (50°–80°) attitude with the prevalent dip in the western–southwestern direction. Locally, the general structure is distorted. For example, the group of slices in the eastern part of the Rymnik zone demonstrates opposite, northeastern dips (Fig. 4a), which indicates intense folding deformations of thick imbricate packets. The structure of this accretionary wedge segment is additionally complicated by counterclockwise rotation of several slices up to their near-latitudinal and northeastern strikes (Fig. 4a), presumably in response to sinistral shear dislocations. Tectonic slices are also displaced along variably oriented faults; such a situation determines their irregular arrangement and relations between each other.

The tectonic slices differ in dislocation patterns of their internal structure. The slices of oceanic sediments several tens of meters thick are usually composed of uniform rocks: cherts or siliceous mudstones. They are usually characterized by a simple homoclinal structure with bedding oriented parallel to bordering tectonic faults. The rocks demonstrate scaly cleavage, which is of variable intensity, oriented parallel to the bedding, and has developed in some zones of the slice or through its whole section. The thicker (50–400 m) slices composed of cherts, basalts, and siliceous (siliceous–tuffaceous) mudstones are characterized by a more complex internal structure. Some cherts have

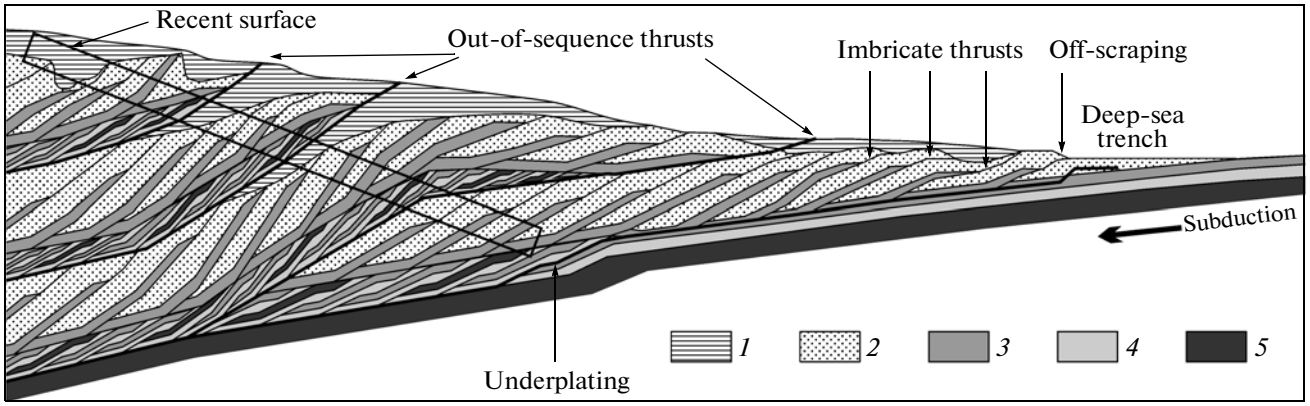

Fig. 5. The idealized formation model of the East Sakhalin accretionary wedge, modified after [41, 50, 51].
(*1*) draping sediments; (*2*) trench-fill turbidites; (*3*) hemipelagic deposits; (*4*) pelagic deposits; (*5*) ocean-floor basalts.

deformed into narrow isoclinal and asymmetrical folds with differently oriented hinges. Other cherty slices or their fragments are divided by frequent intercrossing faults into a system of lenses decimeters to meters thick, deformed, with complex interrelations. Such a lenticular structure is even more complex in fragments of slices composed of alternating cherts and basalts. The lenses of cherts and basalts are frequently mixed with each other up to a chaotic state and their section acquires a melange appearance. Locally, chloritized basalts form a matrix with lenses and blocks of cherts and basalts. In other slices, such a fragmented and mixed texture involves also cherts and tuffaceous–siliceous mudstones with some intensely foliated tuffaceous–siliceous mudstones constituting the groundmass.

Most of the slices composed of mudstones and trench-fill turbidites (100–900 m thick) are characterized by homoclinal structure with insignificant variations in the directions and dip angles of the bedding planes. Some of them have deformed into rare isoclinal folds, which are recognizable owing to replacement of the normal attitude by an overturned one. The variably intense cleavage, both scaly and plane-parallel, is mostly developed in mudstones and thin turbidites. It is oriented parallel to bedding planes, demonstrates zoning patterns, and is confined in many slices to their tectonic borders.

The slices composed of draping sediments (chaotic deposits of debris flows and intervening stratified members) are variable in the thickness from a hundred of meters to several kilometers. Their internal structure is also variable. The slices several hundreds of meters thick are subordinate to the general structure (Figs. 3, 4). They are either homoclinal or deformed into isoclinal folds, which are recognizable owing to the replacement of the normal attitude by the overturned one. The scaly cleavage is characterized by zoned patterns being highly variable in intensity and orientation ordering.

The slices, several kilometers thick, observed in the western part of the Nabil zone (Fig. 3c) and central part of the Rymnik zone (Fig. 4b) contain large and open folds with relatively gentle bends in plan, in addition to fragmentary isoclinal folds. The axial surfaces of these gentle folds are oriented both nearly parallel to the general strike of the structure and notably deviating from the latter. The hinges of many folds dip at significant angles (30°–60°). The folds are disturbed by steep differently oriented faults, displaced fragments of which irregularly join each other. The folds with steeply dipping hinges are formed in response to differently oriented shear displacements. The scaly cleavage shows zoned distribution. Thick slices consisting of the draping sedimentary complex are notable for their large and less ordered folds against the background of the general accretionary wedge structure. It is conceivable that such slices and their groups represent deformed fragments of narrow sedimentation basins developed on the slopes of the accretionary wedge.

Differences in the composition and structure of slices probably reflect the different ways of their involvement in the accretionary wedge structure. The formation of accretionary wedges is usually thought to be related to two processes: (1) off-scraping and (2) underplating [46, 50, 51]. The first process determines the lateral growth of the wedge owing to successive accretion of new tectonic slices to its frontal part along surfaces of imbricate thrusts. The second process is responsible for the increase in wedge thickness by the accretion of tectonic slices in the form of duplexes to its base. The off-scraped slices are composed of sediments constituting upper parts of the downgoing slab (mostly trench-fill turbidites), while tectonically underplated fragments include lower parts of the sedimentary complex and ocean-floor basalts. It is assumed that the thickness of the wedge in its rear part increases owing to the juxtaposition of off-scraped and tectonically underplated fragments of the sedimentary complex along major out-of-sequence thrusts [41].

Table 1. Radiolarians identified in samples from the Nabil zone

Species \ Sample	500	500-1	500-2	501-1	501-3	501-4	502-2	502-3	503	640-2	640-3	641-1	644-1	652-1	652-2	652-3	654-1	656-1	656-2	656-3	657-1	657-2	658-1	661.2	662-1	662-2	668-1	668-3	673-1	673-2	679-1	679-2	681-1	681-2	692-2	695-1	695-2	695-3	695-4	696-1	699-2	702-2	706-1	706-3	713-1	718-2	721-1	722-1	723-1	724-1	725-1	725-2	738-2	741-1
Acaeniotyle diaphorogona Foreman																																																							
Acaeniotyle glebulosa (Foreman)																																																						
Acaeniotyle longispina (Squinabol)																																																						
Acaeniotyle macrospina (Squinabol)																																																						
Acaeniotyle umbilicata (Rust)																																																						
Acanthocircus multidentatus (Squinabol)																																																						
Archaeocenosphaera ?mellifera O'Dogherty																																																						
Becus helenae (Schaaf)																																																						
Becus horridus (Squinabol)																																																						
Becus sp. cf. *B. regius* O'Dogherty																																																					
Crolanium puga (Schaaf)																																																						
Crolanium sp. aff. N spineum (Pessagno)																																																					
Crolanium triangulare (Aliev)																																																						
Crucella ?elisabethae (Rust)																																																					
Crucella euganea (Squinabol)																																																						
Crucella hispana O'Dogherty																																																					
Crucella messinae Pessagno																																																					
Cryptamphorella clivosa (Aliev)																																																					
Cryptamphorella gilkeyi (Dumitrica)																																																					
Dactyliodiscus cayeuxi Squinabol																																																					
Dactyliodiscus lenticulatus (Jud)																																																					
Dactyliosphaera acutispina (Squinabol)																																																					
Dactyliosphaera lepta (Foreman)																																																					
Dactyliosphaera maxima (Pessagno)																																																					
Diacanthocapsa fossilis (Squinabol)																																																					
Dicroa rara (Squinabol)																																																					
Dictyomitra communis (Squinabol)																																																					
Dictyomitra depressa (Baumgartner)																																																					
Dictyomitra excellens (Tan)																																																					
Dictyomitra gracilis (Squinabol)																																																					
Dictyomitra montisserei (Squinabol)																																																					
Dispongotripus acutispinus Squinabol																																																					
Dorypyle communis (Squinabol)																																																					
Emiluvia chica Foreman																																																					
Godia coronata (Tumanda)																																																					
Godia decora (Li & Wu)																																																					
Godia pelta O'Dogherty																																																					
Halesium nevianii (Squinabol)																																																					
Hexapyramis sp. aff. *H. pantanellii* Squinabol																																																					
Hexapyramis precedis Jud																																																					
Hiscocapsa asseni (Tan)																																																					
Hiscocapsa grutterinki (Tan)																																																					
Hiscocapsa kaminogoensis (Aita)																																																					
Hiscocapsa orca (Foreman)																																																					
Hiscocapsa uterculus (Parana)																																																					
Holocryptocanium barbui Dumitrica																																																					
Obeliscoites giganteus (Aliev)																																																					
Obeliscoites perspicuus (Squinabol)																																																					
Pantanellium lanceola (Parana)																																																					
Parvicingula boesii (Parana)																																																					
Parvicingula cosmoconica (Foreman)																																																					
Pessagnobrachia dalpiazzi (Squinabol)																																																					
Pessagnobrachia fabianii (Squinabol)																																																					
Pessagnobrachia irregularis (Squinabol)																																																					
Phalangites calamus O'Dogherty																																																					

Note: Samples 725-1, 725-2, 738-2, and 741-1 were taken in separate exposures along the Ivashka River (Fig. 2, profile 2a).

Table 1. (Contd.)

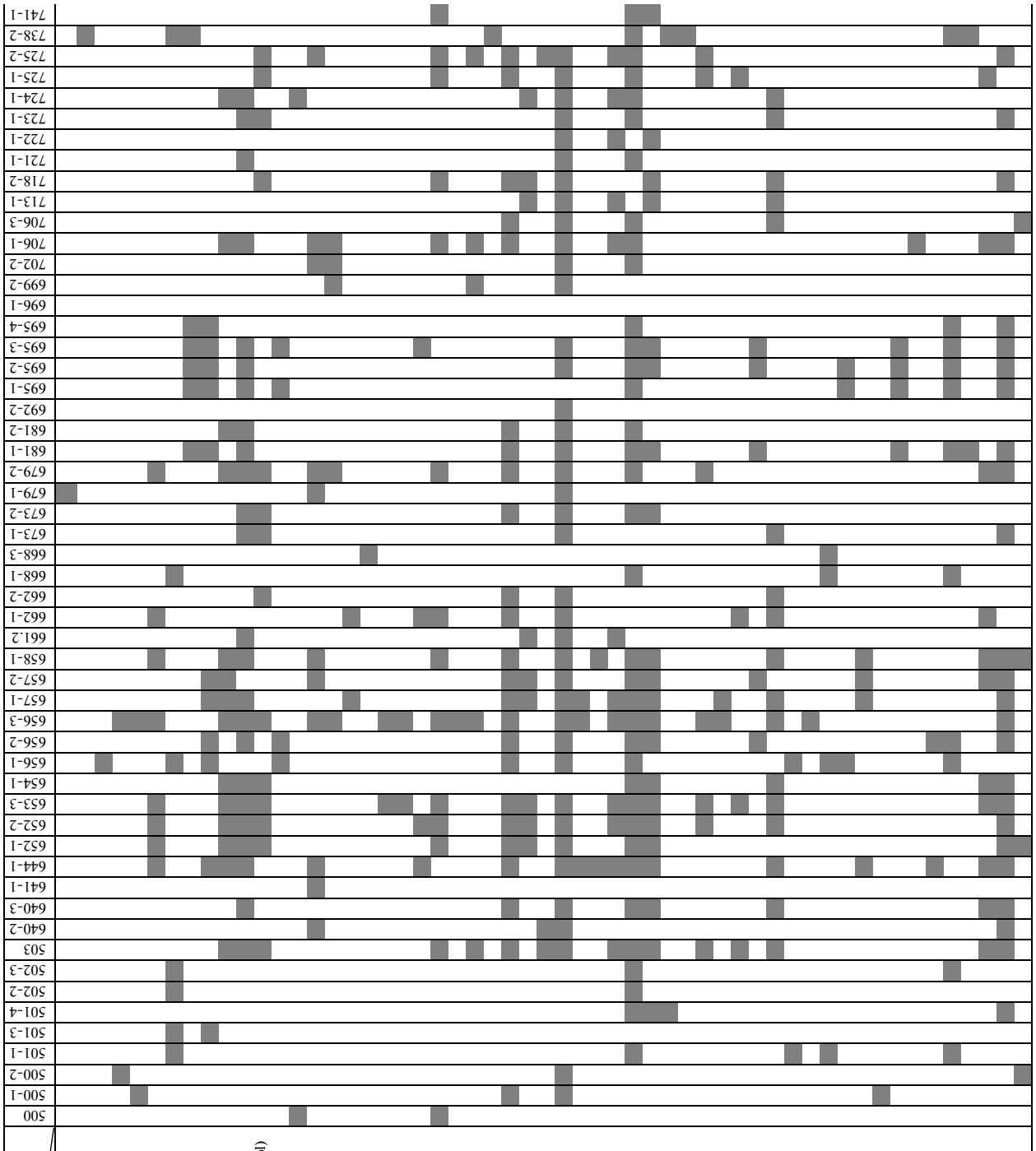

Table 2. Radiolarians identified in samples from the Rymnik zone

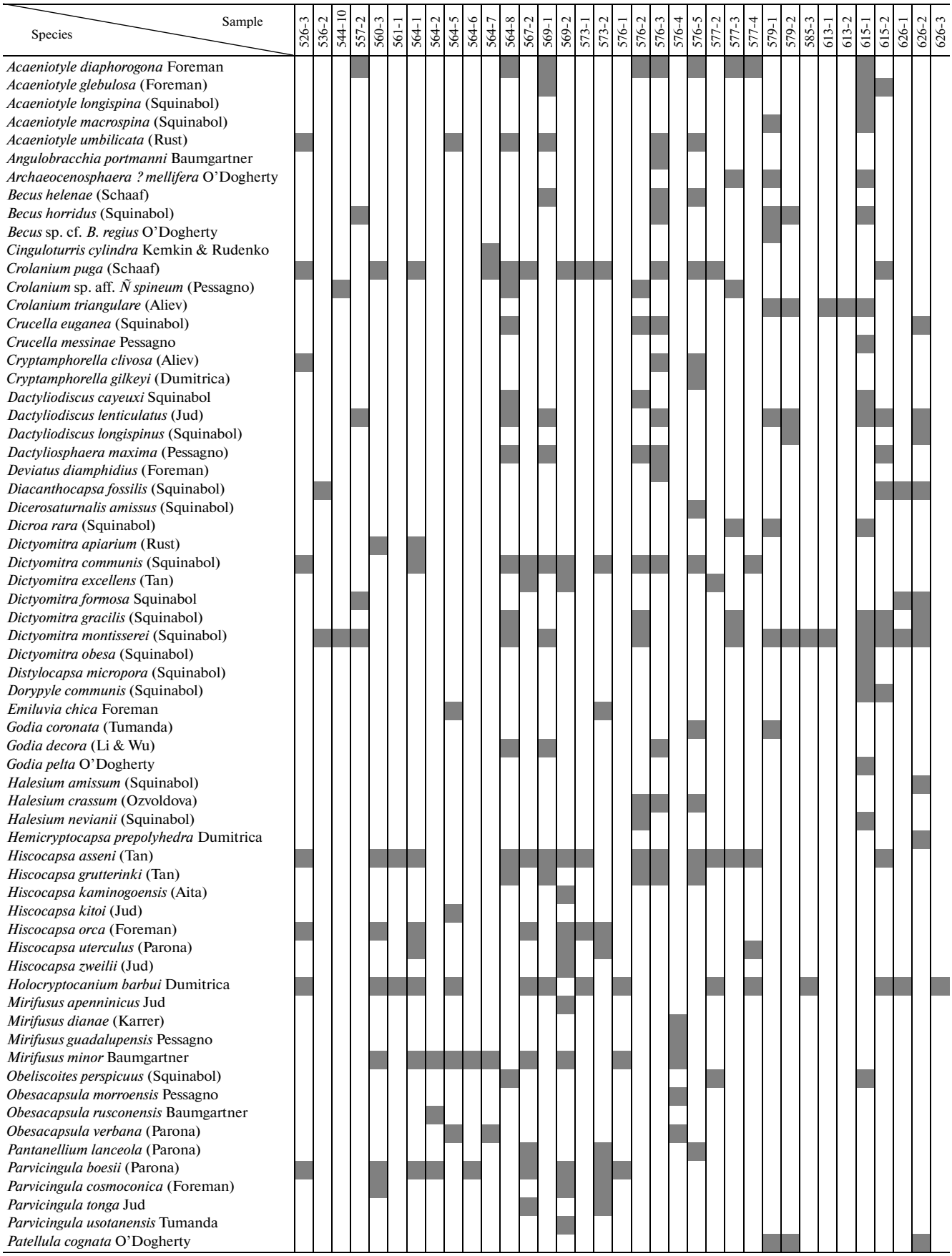

Table 2. (Contd.)

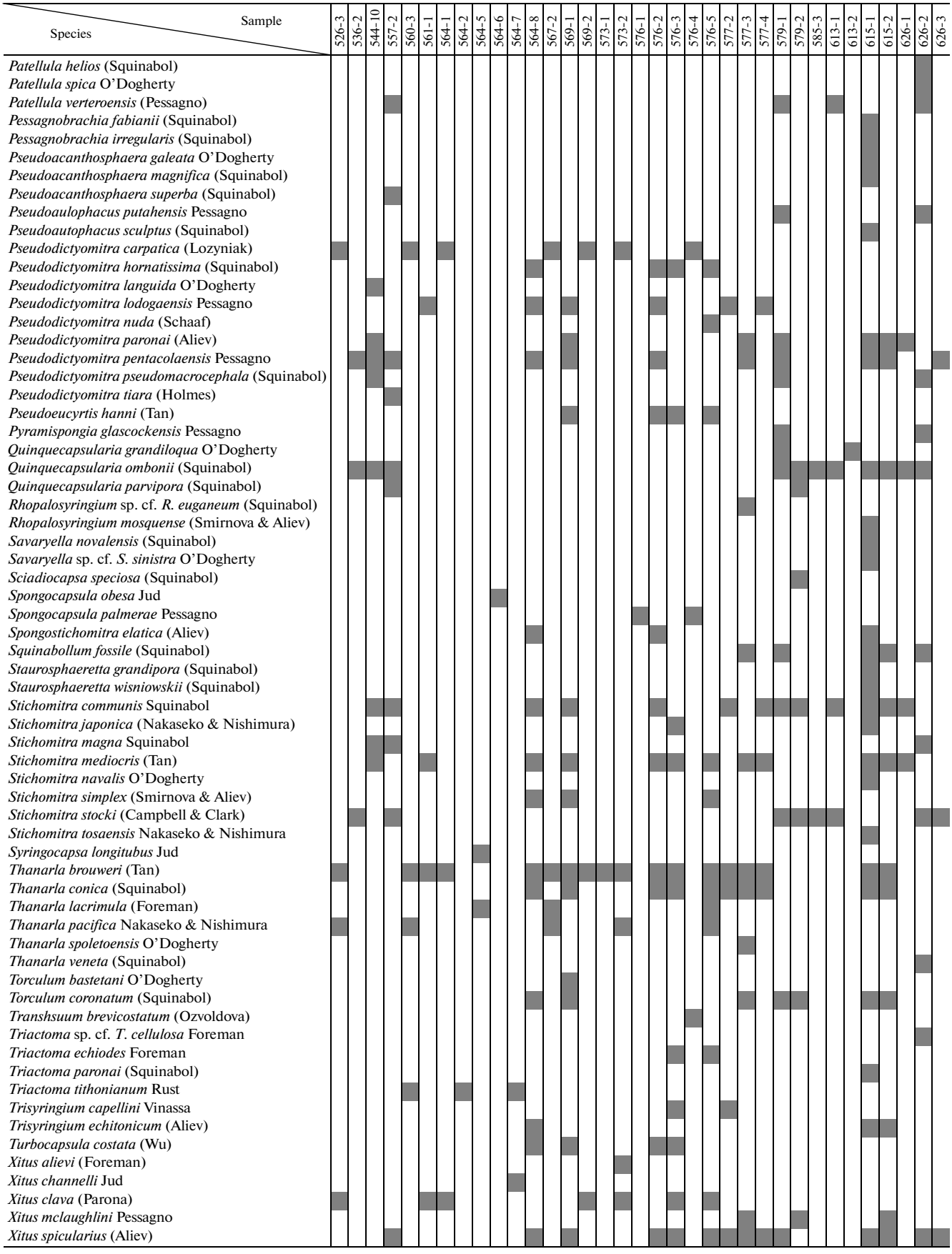

Plate 1

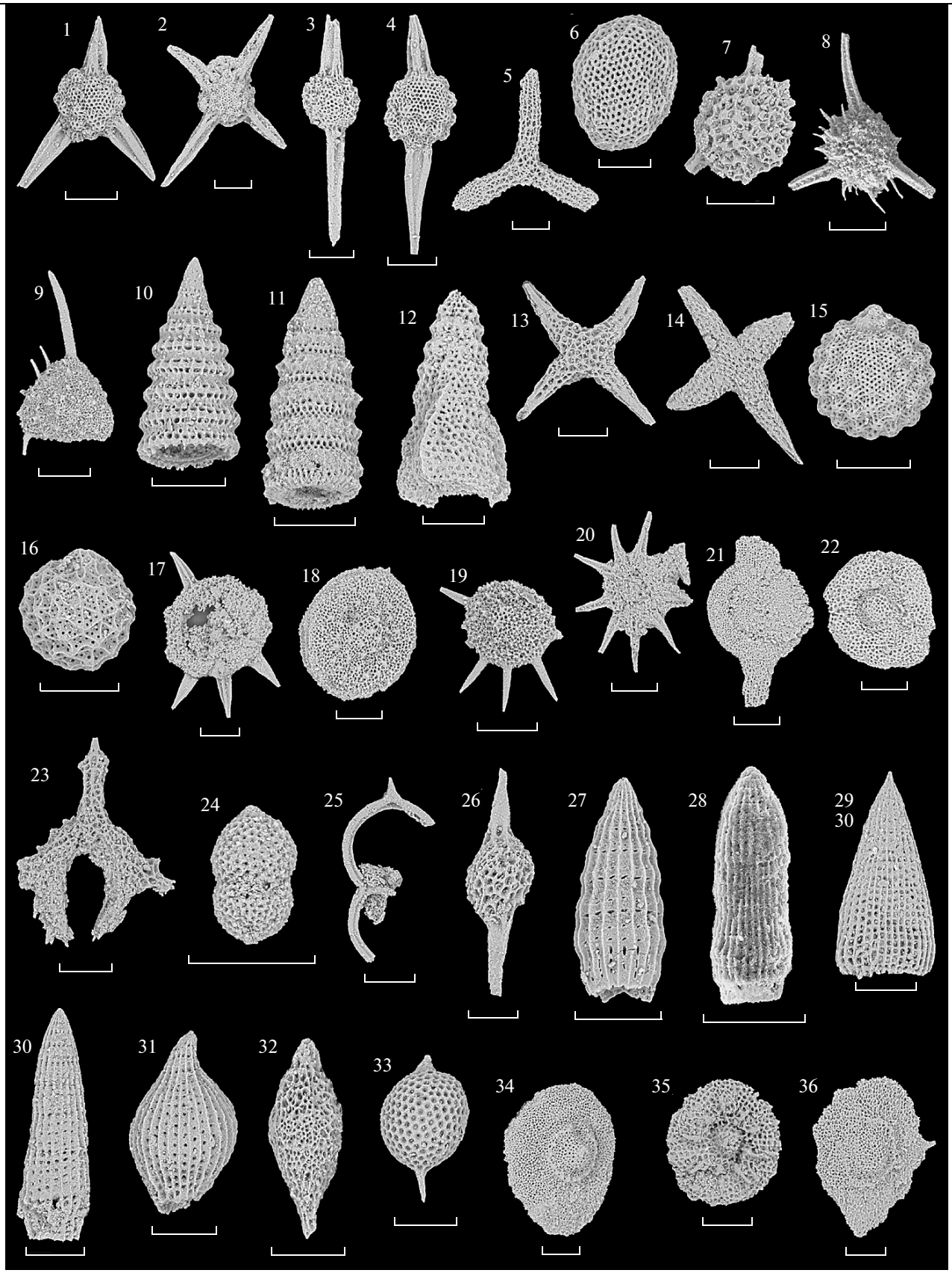
1
2
3
4
5
6
7
8
9
10
11
12
13
14
15
16
17
18
19
20
21
22
23
24
25
26
27
28
29
30
30
31
32
33
34
35
36

Plate 1. Radiolarians from the central part of the East Sakhalin accretionary wedge. Numbers after species names designate samples. The scale bar is 100 μm.

(1) *Acaeniotyle diaphorogona* Foreman, 564-8; (2) *Acaeniotyle glebulosa* (Foreman), 679-2; (3) *Acaeniotyle longispina* (Squinabol), 658-1; (4) *Acaeniotyle umbilicata* (Rüst), 576-3; (5) *Angulobracchia portmanni* Baumgartner, 576-3; (6) *Archaeocenosphaera ? mellifera* O'Dogherty, 615-1; (7) *Becus helenae* (Schaaf), 576-3; (8) *Becus horridus* (Squinabol), 615-1; (9) *Becus* sp. cf. *B. regius* O'Dogherty, 579-1; (10) *Crolanium puga* (Schaaf), 644-1; (11) *Crolanium* sp. aff. *C. spineum* (Pessagno), 657-1; (12) *Crolanium triangulare* (Aliev), 662-1; (13) *Crucella euganea* (Squnabol), 564-8; (14) *Crucella messinae* Pessagno, 615-1; (15) *Cryptamphorella clivosa* (Aliev), 576-5; (16) *Cryptamphorella gilkeyi* (Dumitrica), 576-5; (17) *Dactyliodiscus cayeuxi* Squinabol, 644-1; (18) *Dactyliodiscus lenticulatus* (Jud), 579-1; (19) *Dactyliodiscus longispinus* (Squinabol), 626-2; (20) *Dactyliosphaera acutispina* (Squinabol), 706-1; (21) *Dactyliosphaera lepta* (Foreman), 662-1; (22) *Dactyliosphaera maxima* (Pessagno), 656-3; (23) *Deviatus diamphidius* (Foreman), 576-3; (24) *Diacanthocapsa fossilis* (Squinabol), 536-2; (25) *Dicerosaturnalis amissus* (Squinabol), 576-3; (26) *Dicroa rara* (Squinabol), 577-3; (27) *Dictyomitra communis* (Squinabol), 576-5; (28) *Dictyomitra excellens* (Tan), 569-2; (29) *Dictyomitra gracilis* (Squinabol), 657-1; (30) *Dictyomitra montisserei* (Squinabol), 725-2; (31) *Dictyomitra obesa* (Squinabol), 615-1; (32) *Distylocapsa micropora* (Squinabol), 615-1; (33) *Dorypyle communis* (Squinabol), 615-1; (34) *Godia coronata* (Tumanda), 579-1; (35) *Godia decora* (Li & Wu), 576-3; (36) *Godia pelta* O'Dogherty, 656-3.

As for the examined part of the accretionary wedge, we can only assume the juxtaposition of both off-scraped and tectonically underplated fragments in its present-day structure (Fig. 5). Their reliable recognition is complicated by significant changes of the initial accretionary structure in the course of long evolution of the wedge and its post-accretionary transformation. For the slices composed of turbidites, off-scraping is the most probable process. Similar process presumably also controlled the accretion of slices, in which siliceous and tuffaceous–siliceous mudstones are overlain by mudstones deposited in the deep-sea trench. Slices composed of cherts and basalts were, probably, tectonically underplated to the base of the wedge, which was also assumed by previous researchers for the Nabil zone in the area under consideration [49]. Their subsequent juxtaposition with off-scraped slices is assumed for the continued thrusting in the rear part of the wedge, where draping deposits, which are tectonically juxtaposed in the present-day accretionary wedge with different accreted slices, are presumably also involved into the imbricate structure (Fig. 5).

AGE AND STRATIGRAPHY OF SEDIMENTARY COMPLEXES

The sedimentary sections involved in the imbricate structure of the Nabil and Rymnik zones are incomplete and were significantly disturbed during both accretion and subsequent tectonic transformations. Reconstructions of initial stratigraphic successions based on individual fragments of them in different tectonic slices proved possible only owing to finds of fossil radiolarians, which constrained the ages of host formations.

For radiolarian analysis, approximately 180 samples were taken from cherts, siliceous and tuffaceous–silicieous mudstones, and siliciclastic mudstones from different detrital deposits. Radiolarians were extracted with a 1–4% solution of hydrofluoric acid. Over 80 samples yielded well-preserved radiolarian assemblages, which allowed the ages of host rocks to be determined with variable reliability. The position of samples with indication of their ages is shown in schematic route geological maps (Figs. 3, 4). Tables 1 and 2 present identified radiolarian species (according to taxonomic nomenclature in [57]) and Plates 1–3 illustrate SEM images of most of them.

The biostratigraphic scale of unitary associations [58] that unites scales proposed in [47] and [57] was used for determining age of Cretaceous radiolarian assemblages. The defined radiolarian assemblages are correlated with this scale by the method of unitary associations [45] using the BioGraph software [61]. From the technical viewpoint, radiolarian assemblages with the corresponding digital codes were processed together with the digital database of the applied biostratigraphic scale. The taxa determined in the open nomenclature (cf. and aff.) were omitted from correlation. The software algorithm yielded the succession of 69 unitary associations, which include 16 new (in addition to 53 in the initial scale) associations. The modified succession was correlated with the initial scale [58] as well as with scales in [47] and [57]. The resulting data are presented in form of a plot (Fig. 6), where the ages are grouped for sediment types and arranged (from left to right) according to the relative position of dated samples along the profile across the accretionary wedge (from the west to east). The age of two Jurassic radiolarian assemblages (chert samples 576-1 and 576-4 from the Rymnik zone) is determined in the zonal scale of unitary associations UAZ95 [38] and projected at the applied scale [58].

In the **Nabil zone**, the age of cherts is estimated to range from Tithonian–Valanginian to Barremian, and that of siliceous and tuffaceous–siliceous mudstones corresponds to the early Aptian–middle Albian. The age of turbidites in the eastern part of the zone has been determined as middle–late Albian similarly to that for the draping sedimentary complex in its western part. Limestones from two slices in the western zone correlate with the late Albian judging from the late Aptian age of overlying (probably, with a significant hiatus) siliceous mudstones.

In the **Rymnik zone**, the ages of cherts range from late Kimmeridgian–early Tithonian to early Aptian. Ages obtained for siliceous and tuffaceous–siliceous mudstones are scattered within middle Aptian–Cen-

Plate 2

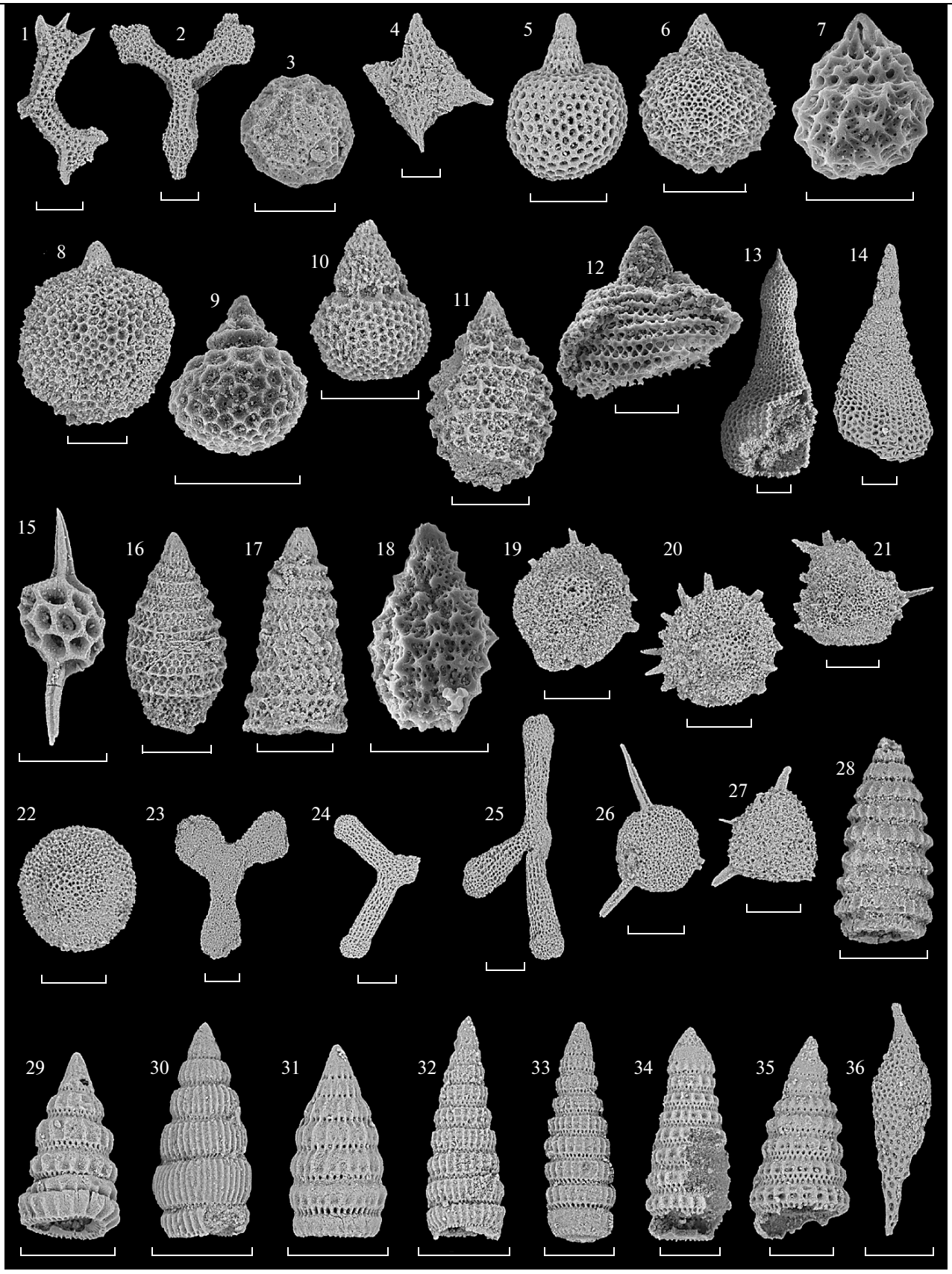
1
2
3
4
5
6
7
8
9
10
11
12
13
14
15
16
17
18
19
20
21
22
23
24
25
26
27
28
29
30
31
32
33
34
35
36

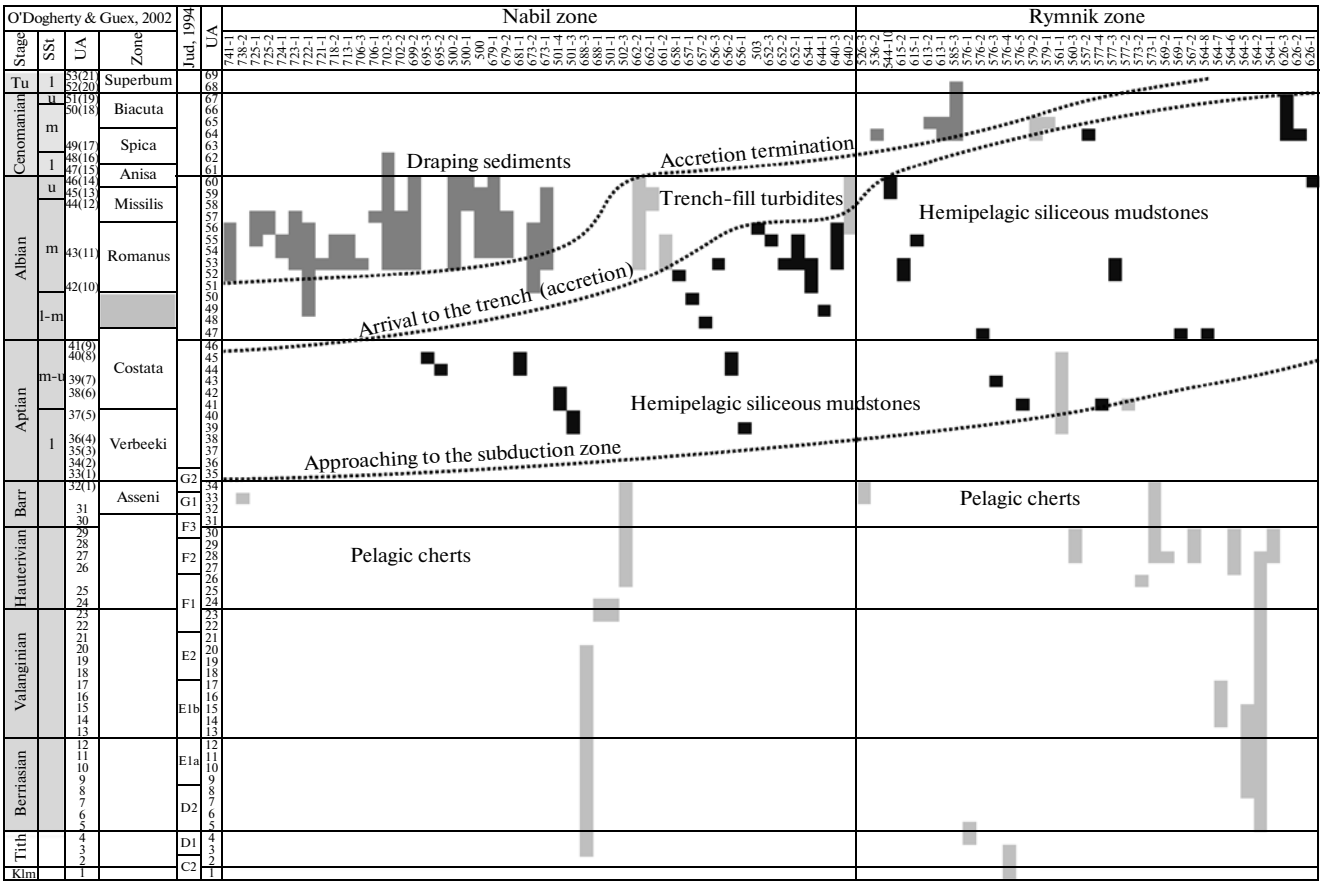

Fig. 6. Ages of sediments from the central part of the East Sakhalin accretionary wedge in the scale of unitary associations (UA). Ages are grouped according to sediment types and arranged (from left to right) in line with relative position of dated samples across the accretionary wedge from the west eastward. The obtained succession of unitary associations UA 1–69 correlates with the initial unitary scale UA 1–53, O'Dogherty and Guex, 2002[58] (shown in brackets are unitary associations UA 1–21 of the scale of O'Dogherty, 1994 [57]) and with the scale of Jud, 1994 [47]. Dotted lines designate stratigraphic boundaries of different-facies deposits with indication of their paleogeographic interpretation. Ages of samples 576-1 and 576-4 (cherts from the Rymnik zone) are determined in the scale UAZ95 [38] and projected on the used UA scale. Samples 725-1, 725-2, 738-2, and 741-1 were taken from isolated outcrops along the Ivashka River (Fig. 2, intersection 2a) southwest of the main route intersection of the Nabil zone.

omanian limits. The turbidites in the eastern part of the zone and draping sediments in its western part are middle Cenomanian in age.

These radiolarian ages made it possible to reconstruct stratigraphic successions beginning with pelagic cherts (with basalts) overlain by hemipelagic siliceous and tuffaceous–siliceous mudstones, which are replaced higher in the section by terrigenous detrital deposits that include trench-fill turbidites and draping sediments. Poor preservation of radiolarians prevented

Plate 2. Radiolarians from the central part of the East Sakhalin accretionary wedge. Numbers after species names designate samples. The scale bar is 100 μm.

(1) *Halesium amissum* (Squinabol), 626-2; (2) *Halesium crassum* (Ozvoldova), 576-3; (3) *Hemicryptocapsa prepolyhedra* Dumitrica, 626-2; (4) *Hexapyramis* sp. aff. *H. pantanellii* Squinabol, 656-3; (5) *Hiscocapsa asseni* (Tan), 576-3; (6) *Hiscocapsa grutterinki* (Tan), 644-1; (7) *Hiscocapsa kaminogoensis* (Aita), 569-2; (8) *Hiscocapsa orca* (Foreman), 569-2; (9) *Hiscocapsa uterculus* (Parona), 569-2; (10) *Hiscocapsa zweilii* (Parona), 569-2; (11) *Mirifusus apenninicus* Jud, 569-2; (12) *Mirifusus minor* Baumgartner, 569-2; (13) *Obeliscoites giganteus* (Aliev), 644-1; (14) *Obeliscoites perspicuus* (Squinabol), 564-8; (15) *Pantanellium lanceola* (Parona), 576-5; (16) *Parvicingula boesii* (Parona), 569-2; (17) *Parvicingula cosmoconica* (Foreman), 569-2; (18) *Parvicingula usotanensis* Tumanda, 569-2; (19) *Patellula cognata* O'Dogherty, 579-1; (20) *Patellula helios* (Squinabol), 626-2; (21) *Patellula spica* O'Dogherty, 626-2; (22) *Patellula verteroensis* (Pessagno), 579-1; (23) *Pessagnobrachia dalpiazii* (Squinabol), 656-3; (24) *Pessagnobrachia fabianii* (Squinabol), 662-1; (25) *Pessagnobrachia irregularis* (Squinabol), 56-3; (26) *Pseudoaulophacus putahensis* Pessagno, 579-1; (27) *Pseudoaulophacus sculptus* (Squinabol), 658-1; (28) *Pseudodictyomitra carpatica* (Lozyniak), 569-2; (29) *Pseudodictyomitra hornatissima* (Squinabol), 576-3; (30) *Pseudodictyomitra lodogaensis* Pessagno, 564-8; (31) *Pseudodictyomitra nuda* (Schaaf), 576-5; (32) *Pseudodictyomitra paronai* (Aliev), 679-2; (33) *Pseudodictyomitra pentacolaensis* Pessagno, 657-1; (34) *Pseudodictyomitra pseudomacrocephala* (Squinabol), 503; (35) *Pseudodictyomitra tiara* (Holmes), 557-2; (36) *Pseudoeucyrtis hanni* (Tan), 576-3.

Plate 3

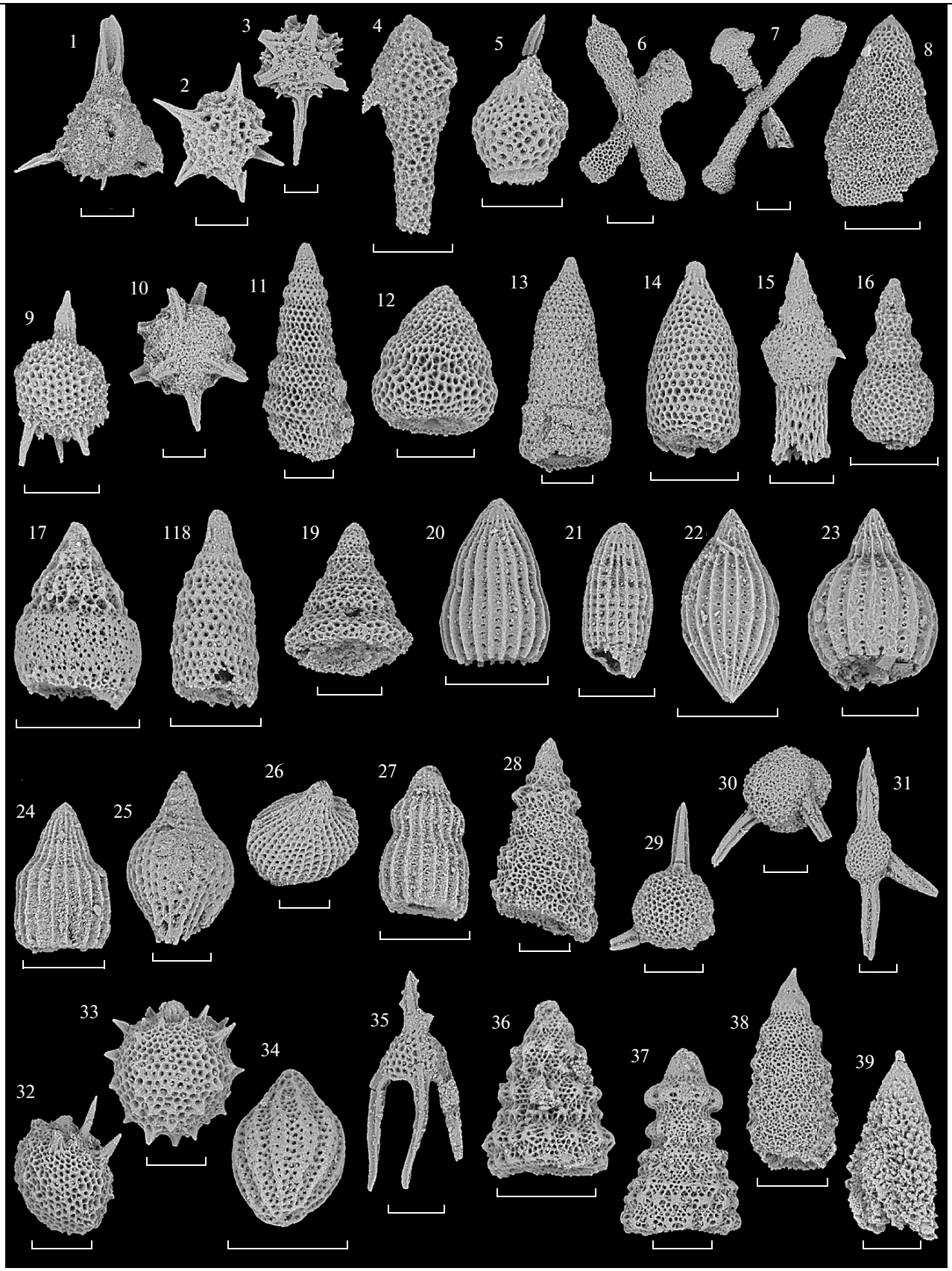
1
2
3
4
5
6
7
8
9
10
11
12
13
14
15
16
17
118
19
20
21
22
23
24
25
26
27
28
29
30
31
32
33
34
35
36
37
38
39

Plate 3. Radiolarians from the central part of the East Sakhalin accretionary wedge. Numbers after species names designate samples. The scale bar is 100 μm.

(1) *Pyramispongia glascockensis* Pessagno, 579-1; (2) *Quinquecapsularia ombonii* (Squinabol), 658-1; (3) *Quinquecapsularia parvipora* (Squinabol), 656-3; (4) *Rhopalosyringium* sp. cf. *R. euganeum* (Squinabol), 577-3; (5) *Rhopalosyringium mosquense* (Smirnova & Aliev), 657-1; (6) *Savaryella novalensis* (Squinabol), 615-1; (7) *Savaryella* sp. cf. *S. sinistra* O'Dogherty, 656-3; (8) *Spongostichomitra elatica* (Aliev), 564-8; (9) *Squinabollum fossile* (Squinabol), 679-2; (10) *Staurosphaeretta wisniowskii* (Squinabol), 725-2; (11) *Stichomitra communis* Squinabol, 658-1; (12) *Stichomitra japonica* (Nakaseko & Nishimura), 576-3; (13) *Stichomitra magna* Squinabol, 725-2; (14) *Stichomitra mediocris* (Tan), 564-8; (15, 16) *Stichomitra navalis* O'Dogherty, 615-1, 656-3; (17) *Stichomitra simplex* (Smirnova & Aliev), 576-5; (18) *Stichomitra stocki* (Campbell & Clark), 557-2; (19) *Stichomitra tosaensis* Nakaseko & Nishimura, 615-1; (20) *Thanarla brouweri* (Tan), 564-8; (21) *Thanarla conica* (Squinabol), 658-1; (22) *Thanarla lacrimula* (Foreman), 576-5; (23) *Thanarla pacifica* Nakaseko & Nishimura, 576-5; (24) *Thanarla pulchra* (Squinabol), 679-2; (25, 26) *Thanarla spoletoensis* O'Dogherty, 656-3; (27) *Thanarla veneta* (Squinabol), 503; (28) *Torculum coronatum* (Squinabol), 615-1; (29) *Triactoma* sp. cf. *T. cellulosa* Foreman, 626-3; (30) *Triactoma echiodes* Foreman, 576-3; (31) *Triactoma paronai* (Squinabol), 615-1; (32) *Trisyringium capellini* Vinassa, 576-3; (33) *Trisyringium echitonicum* (Aliev), 644-1; (34) *Turbocapsula costata* (Wu), 564-8; (35) *Ultranopora praespinifera* Pessagno, 644-1; (36) *Xitus clava* (Parona), 576-5; (37) *Xitus mclaughlini* Pessagno, 644-1; (38) *Xitus spicularius* (Aliev), 644-1; (39) *Xitus spinosus* (Squinabol), 658-1.

reconstruction of more complete stratigraphic successions and determination of exact positions of basalts in them.

In the W–E direction, the accretionary wedge demonstrates distinct rejuvenation of different-facies sedimentary units and their boundaries from its rear part to the front, owing to which underlying sediments successively occupy stratigraphic levels of westerly located overlying strata (Fig. 6). The particularly distinct diachronic behavior is characteristic of the boundary between hemipelagic and siliciclastic deposits, which becomes younger from the Aptian–Albian transition in the western part of the Nabil zone to the middle (late?) Cenomanian in the eastern part of the Rymnik zone.

The reconstructed stratigraphic successions (Fig. 7) differ from the stratigraphic models available for the Nabil and Rymnik zones by the successive replacement of different-facies sediments without their reiteration in the section. The obtained ages indicate a lack of post-Albian sediments in the Nabil zone, which is inconsistent with the late Albian–early Cenomanian and late Cenomanian–early Turonian ages inferred from the radiolarian assemblages for the Ostraya and Khoi formations, respectively [16]. This is explained by both the application of a more advanced biostratigraphic scale and more reliable identification of volumetric radiolarian specimens extracted from host rocks. Views on the stratigraphy of the Rymnik zone have changed substantially. It appears that it includes Upper Jurassic, Lower Cretaceous, and Cenomanian deposits and lacks younger strata. The Late Cretaceous (Coniacian (?)–Santonian to Maastrichtian (Danian?) age of the Rymnik Group was substantiated earlier by finds of faunal remains in the easternmost part of the zone and extrapolated into deposits beyond its limits.

SEDIMENTATION AND ACCRETION HISTORY

The obtained data make it possible to reconstruct the formation history of sediments on the oceanic plate and convergent boundary and to determine their accretion age. The reconstructed successions (Fig. 7) are typical of Mesozoic accretionary wedges [17, 46, 54, 55]. Such successions composed of cherts, siliceous mudstones, and detrital sediments of the deep-sea trench (chert–clastic sequence [55]) reflect sedimentation on the moving oceanic plate since its formation in the spreading zone to its subsidence in the subduction zone [46, 54, 55].

The stratigraphic successions of the Nabil and Rymnik zones in the East Sakhalin accretionary wedge record a significant part of the sedimentation history on the Izanagi oceanic plate, which existed in the Northwest Pacific at that time and moved in the N–NW direction [42, 53]. Pelagic siliceous sedimentation was in progress since the Kimmeridgian–Tithonian till Barremian–Aptian with the formation of volcanic edifices composed of basalts and crowned by limestones in some areas of the plate. Hemipelagic sedimentation started in the early Aptian reflecting an approach of the oceanic plate to the convergent boundary; the slightly earlier commencement of this process is recorded in the accreted deposits of the Nabil zone. Termination of hemipelagic sedimentation in the different areas of the Izanagi Plate occurred in the period lasting from the terminal Aptian to middle–late Cenomanian. The presence of the pyroclastic component and numerous tuff beds among hemipelagic sediments indicates simultaneous explosive volcanism at the convergent plate boundary. The volcanic activity is probably related to the development of the Moneron–Rebun–Kabato and Kem–Samarga fragments of the volcanic arc in the Aptian–Albian and the initiation of the Sikhote Alin volcano-plutonic belt formation in the Cenomanian.

The onset of turbidite accumulation reflects the arrival of the oceanic plate to the deep-sea trench, thus indicating the beginning of accretionary events [46, 55]. Ages of turbidites determined in two tectonic slices reflect the middle–late Albian and middle Cenomanian accretion episodes for the eastern parts of the Nabil and Rymnik zones, respectively. Fragments of hemipelagic sections and draping sediments may be

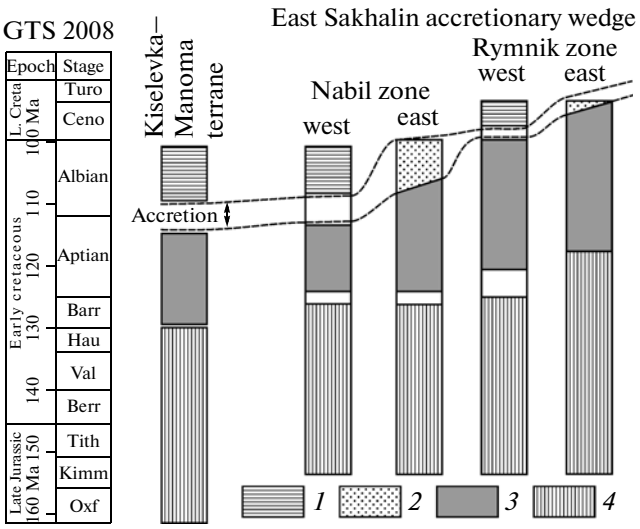

Fig. 7. Correlation between stratigraphic successions of the Kiselevka–Manoma terrane and East Sakhalin accretionary wedge and their accretion events in the geological time scale (GTS 2008) [59]. (*1*) draping sediments; (*2*) trench-fill turbidites; (*3*) hemipelagic siliceous and tuffaceous–siliceous mudstones; (*4*) pelagic cherts (with basalts).

used for accretion timing as well. Accumulation of youngest hemipelagic sediments immediately precedes accretion and formation of the draping complex marks its terminal phase. Taking into consideration all the obtained age estimates, one may conclude that accretion was in progress in the period since the terminal Aptian till middle Albian in the western part of the Nail zone and in the middle–late Albian in its eastern part (Fig. 7). Slices of the western and eastern parts of the Rymnik zone were accreted in the early Cenomanian (by the middle Cenomanian) and middle Cenomanian, respectively (Fig. 7). The easternmost fragments of the Rymnik zone were accreted after the middle–late Cenomanian, since they include corresponding hemipelagic sediments. The fragment of the accretionary wedge ~35 km wide in its present-day structure was formed during the Albian–Cenomanian period lasting ~18 myr. The accretion rate of the accretionary wedge is estimated to be ~2 km/myr, which represents a minimal value of off-scraping accretion without account for the subsequent shortening of the wedge.

The formation of the Nabil zone of the accretionary wedge in East Sakhalin in the Middle–Late Albian terminated the island-arc development stage of the Sikhote Alin–Sakhalin accretionary system. The accretion of the Rymnik zone, which continued in the Cenomanian, corresponds to the initiation of the East Sikhote Alin volcanogenic belt and transformation of the accretionary system into the continental-marginal one. These events only partially reflect a long development history of the East Sakhalin accretionary wedge.

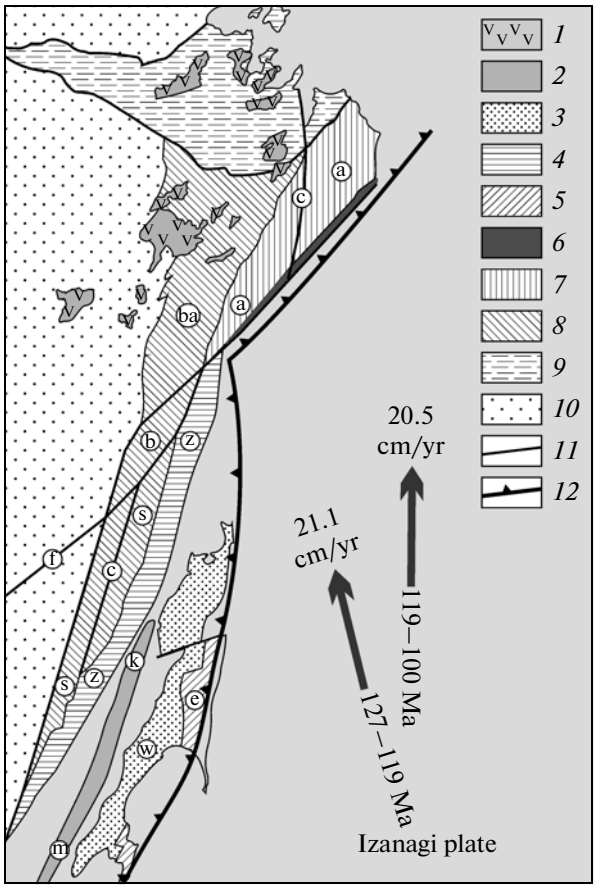

Fig. 8. Paleotectonic reconstruction of the position of the accretionary wedges of the Kiselevka–Manoma terrane and East Sakhalin in early Albian. The directions and rates of the movement of the Izanagi plate relative to Eurasia according to [53]. (*1*) Early–Late Cretaceous Khingan–Okhotsk volcanic belt; (*2*) Early Cretaceous island arc with its fragments: Kema–Samarga (k) and Moneron–Rebun–Kabato (m); (*3*) fore-arc trough of West Sakhalin (w); (*4*) Early Cretaceous Zhuravlevka turbidite trough, (*5–8*) acccretionary wedges: (*5*) Aptian–Albian East Sakhalin (e), (*6*) Aptian–Albian, Kiselevka–Manoma terrane (a), (*7*) Early Cretaceous, Amur terrane; (*8*) Jurassic–Early Cretaceous, Badzhal (ba), Bikin (b), and Samarka (s) terranes, (*9*) Mongol–Okhotsk suture, (*10*) cratonic areas, (*11*) large faults, including traces of future Central Sikhote Alin (c) and Fushun–Mishan (f); (*12*) subduction zone.

The obtained age estimates are of significance for correlation of accretionary wedges in the eastern Asian continent and paleotectonic reconstructions. Age of the accretion in the western part of the Nabil zone corresponds to that of the Kiselevka–Manoma terrane (late Aptian–early Albian) located on the continent [15]. Despite differences in the composition of accreted deposits, their stratigraphic successions demonstrate significant similarity: synchronous onset and termination of hemipelagic sedimentation. The new data on the accretion timing in the Nabil zone confirm the previous assumption on the synchronous formation of some fragments of the East Sakhalin and Kiselevka–Manoma accretionary wedges [15, 62].

The model of a single convergent boundary with the position of elements of the Sakhalin accretionary system south of their present-day location is the simplest paleotectonic reconstruction that explains the synchronous accretion (Fig. 8). Such a position of Sakhalin's tectonic elements was reconstructed earlier as well [62], although in a slightly different framing of the Sikhote Alin terranes.

CONCLUSIONS

This investigation of a fragment of the accretionary wedge in the central part of the East Sakhalin Mountains made it possible to substantially specify their formation history and to determine the age of accretion episodes. The Nabil zone was accreted in the Albian, and a significant segment of the Rymnik zone, in the Cenomanian. The western part of the Rymnik zone formed synchronously with the accretionary wedge of the Kiselevka–Manoma terrane located on the continent. It is assumed that these accretionary wedges formed along a single convergent boundary with the location of the Sakhalin accretionary system in the Albian considerably south of its present-day position.

ACKNOWLEDGMENTS

I am grateful to A.A. Konovalenko and V.G. Gal'versen, geologists from the Sakhalin geological prospecting expedition, for their help in conducting field investigations in the East Sakhalin Mountains, and to L.O. Dogherty for permission to use his database on Cretaceous radiolarians. I thank also reviewers V.S. Vishnevskaya, N.Yu. Bragin, and B.A. Natal'in for their constructive comments, which contributed a great deal to improving the manuscript.

REFERENCES

1. N. Yu. Bragin, *Radiolarians in the Lower Mesozoic Sequences of the Eastern USSR* (Nauka, Moscow, 1991) [in Russian].
2. V. S. Vishnevskaya, N. A. Bogdanov, and D. V. Kurilov, "First Finds of Reliable Lower Cretaceous (Berriasian and Valanginian) Radiolarian Assemblages in Eastern Sakhalin," Dolk. Earth Sci. **389** (5), 653–656 (2003) [Dokl. Earth Sci. **389**, 334–337 (2003)].
3. V. S. Vishnevskaya, N. A. Bogdanov, and D. V. Kurilov, "First Data on Barremian–Aptian Radiolarians of Eastern Sakhalin," Dolk. Akad. Nauk **392** (6), 787–791 (2003) [Dokl. Earth Sci. **392**, 1077–1081 (2003)].
4. *Geological Map of Sakhalin. 1 : 1000000. Geology of USSR. Suppl. Vol. 33* Ed. by V. N. Vereshchagin (Mingeo SSSR, Moscow, 1970) [in Russian].
5. *Geology of USSR. Vol. 33. Sakhalin Island. Geological Description*, Ed. by V. N. Vereshchagin and Yu. M. Kovtunovich (Nedra, Moscow, 1970) [in Russian].
6. V. V. Golozubov, A. I. Khanchuk, I. V. Kemkin, et al., "Sikhote Alin–North Sakhalin Orogenic Belt," in *Geodynamics, Magmatism, and Metallogeny of East Russia,* Ed. by A. I. Khanchuk (Dal'nauka, Vladivostok, 2006), Vol. 1 [in Russian].
7. V. M. Grannik, *Upper Cretaceous Volcanogenic–Sedimentary Units of the East Sakhalin Mountains* (Nauka, Moscow, 1978) [in Russian].
8. V. M. Grannik, *Geology and Geodynamics of the Sea of South Okhotsk Region in the Mesozoic and Cenozoic* (Dal'nauka, Vladivostok, 2008) [in Russian].
10. A. I. Zhamoida, *Biostratigraphy of the Mesozoic Siliceous Sequences of Eastern USSR* (Nedra, Leningrad, 1972) [in Russian].
11. A. E. Zharov, "Accretionary Tectonics and Geodynamics of Southern Sakhalin," Geotektonika, No. 4, 45–63 (2004) [Geotectonics **38**, 277–293 (2004)].
12. A. E. Zharov, *Geological Structure and Cretaceous–Paleogene Geodynamics of Southeast Sakhalin* (Sakhalinsk. kn. izd-vo, Yuzhno-Sakhalinsk, 2004) [in Russian].
13. A. E. Zharov, N. Yu. Bragin, and A. N. Rechkin, "The Cretaceous–Lower Paleogene Stratigraphy of Accretionary Rock Complexes in the Tonino–Aniva Peninsula of Southern Sakhalin," Stratigr. Geol. Korrelyatsiya **13** (1), 87–105 (2005) [Stratigr. Geol. Correlation **13**, 80–98 (2005)].
14. S. V. Zyabrev, A. N. Perestoronin, and A. E. Zharov, "Onset of Terrigenous Sedimentation in the West Sakhalin Fore-Arc Trough as the Detail of the Early History of the Sakhalin and Hokkaido Accretionary System," Tikhookean. Geol. **23** (1), 53–61 (2004).
15. S. V. Zyabrev, M. V. Martynyuk, and E. K. Shevelev, "Southwestern Fragment of the Kiselevka–Manoma Accretionary Complex, Sikhote Alin: Stratigraphy, Subductin Accretion, and Postaccretionary Displacements," Tikhookean. Geol. **24** (1), 45–58 (2005).
16. L. I. Kazintsova, "Radiolarian-Based Age of the Siliceous Sequences of the East Sakhalin Mountains," Tikhookean. Geol., No. 2, 90–96 (1988).
17. I. V. Kemkin, *Geodynamic Evolution of Sikhote Alin and Sea of Japan Region in the Mesozoic* (Nauka, Moscow, 2006) [in Russian].
18. V. P. Klyuev and D. F. Semenov, *Geological Map of USSR. 1 : 200000. Sakhalin Series. Sheet M-54-XVIII. Explanatory Notes* (-, Moscow) [in Russian].
19. E. V. Krasnov and E. O. Savitskii, "Upper Jurassic Corall Reefs of Sakhalin and Hypothesis of the Japanese Islands Drift," Dokl. Akad. Nauk SSSR **209** (3), 659–661 (1973).
20. A. I. Malinovskii, V. V. Golozubov, V. P. Simanenko, and A. N. Mitrokhin, "Kem Terrane (East Sikhote Alin)—a Fragment of the Early Cretaceous Island-Arc System of the Eastern Asian Margin," Tikhookean. Geol. **24** (6), 38–58 (2005).
21. B. A. Natal'in, "Mesozoic Accretionary and Collisional Tectonics of the Southern Russian Far East," Tikhookean. Geol., No. 5, 3–23 (1991).
22. L. M. Parfenov, *Continental Margins and Island Arcs of Mesozoids of Northeast Asia* (Nauka, Novosibirsk, 1984) [in Russian].
23. V. K. Popov, V. P. Simanenko, and V. G. Sakhno, East Sikhote Alin Volcanoplutonic Belt (Late Cenomanian–Maastrichtian). Volcanogenic Rocks, in *Geodynamics, Magmatism, and Metallogeny of Eastern Russia*,

Ed. by, A. I. Khanchuk (Dal'nauka, Vladivostok, 2006), Vol. 1 [in Russian].

24. Yu. N. Raznitsin, "Serpentinite Melange and Olistostrome of the Southeastern Part of the East Sakhalin Mountains," Geotektonika, No. 2, 96–108 (1978).
25. Yu. N. Raznitsin, *Ophiolite Allochthone and Adjacent Depressions on the Western Pacific* (Nauka, Moscow, 1982) [in Russian].
26. A. N. Rechkin, "Pre-Cenozoic Sandstones of the East Sakhalin Mountains," in *Geology, Metallogeny, and Hydrogeology of the Kurile Islands* (DVO RAN, Vladivostok, 1991), pp. 91–98 [in Russian].
27. A. V. Rikhter and N. Yu. Bragin, "Structure and Age of the Volcanogenic–Siliceous Deposits of Sakhalin," Izv. AN SSSR. Seriya Geol, No. 2, 89–95 (1984).
28. A. V. Rikhter, *Structure and Tectonic Evolution of Sakhalin in the Mesozoic* (Nauka, Moscow, 1986) [in Russian].
29. V. S. Rozhdestvenskii, "Lithostratigraphy of the Mesozoic–Paleozoic Deposits of the East Sakhalin Mountains," Tikhookean. Geol., No. 5, 48–58 (1983).
30. V. S. Rozhdestvenskii, "Geodynamic Evolution of the Hokkaido–Sakhalin Fold System," Tikhookean. Geol., No. 2, 76–88 (1993).
31. V. P. Simanenko, "Late Mesozoic Volcanic Arcs of East Sikhote Alin and Sakhalin," Tikhookean. Geol., No. 1, 7–13 (1986).
32. V. P. Simanenko and A. I. Khanchuk, "Cenomanian Volcanism of the Eastern Sikhote Alin Volcanic Belt: Geochemical Features," Geokhimiya, No. 8, 866–878 (2003) [Geochem. Int. **41**, 787–798 (2003)].
33. V. P. Simanenko, A. I. Malinovskii, and V. V. Golozubov, "Early Cretaceous Basalts of the Kem Terrane—A Fragment of the Moneron–Samarga Island-Arc System," Tikhookean. Geol. **23** (2), 30–51 (2004).
34. A. I. Khanchuk, A. P. Nikitina, I. V. Panchenko, et al., "Paleozoic and Mesozoic Guyots of Sikhote Alin and Sakhalin," Dokl. Akad. Nauk SSSR **307** (1), 186–190 (1989).
35. A. I. Khanchuk, I. V. Kemkin, and I. V. Panchenko, "Geodynamic Evolution of Sikhote Alin and Sakhalin in the Paleozoic and Mesozoic," in *Pacific Margin of Asia. Vol. 1. Geology* (Nauka, Moscow, 1989), pp. 218–254 [in Russian].
36. A. I. Khanchuk, Extended Abstract of Doctoral Dissertation in Geology and Mineralogy (GIN RAN, Moscow, 1993).
37. A. I. Khanchuk, "Sakhalin–Kamchatka Orogenic Belt," in *Geodynamic, Magmatism, and Metallogeny of East Russia*, Ed. by A. I. Khanchuk (Dal'nauka, Vladivostok, 2006), Vol. 1 [in Russian].
38. P. O. Baumgartner, L. Dogherty, S. Gorican, et al., "Middle Jurassic To Lower Cretaceous Radiolaria of Tethys: Occurrences, Systematics, Biochronology," Memoires de Geologie (Lausanne) **23**, 1172 (1995).
39. A. H. Bouma, "Fossil Contourites in Lower Niesenflusch, Switzerland," J. Sediment. Petrol. **42** (4), 917–921 (1972).
40. K. M. Brown, A. Mascle, and J. H. Behrmann, "Mechanisms of Accretion and Subsequent Thickening in the Barbados Ridge Accretionary Complex: Balanced Cross Sections across the Wedge Toe," in *Proceedings of the Ocean Drilling Program, Scientific Results*, Ed. by W. R. Winkler (TX, US, College Station, TX, 1990), Vol. 110, pp. 209–227.
42. D. C. Engebretson, A. Cox, and R. G. Gordon, "Relative Motions Between Oceanic and Continental Plates in the Pacific Basin," Geol. Soc. Am. Spec. Paper, 59 (1985).
43. R. V. Fisher, "Features of Coarse-Grained, High-Concentration Fluids and Their Deposits," J. Sediment. Petrol. **41** (4), 916–927 (1971).
44. G. Ghibaudo, "Subaqueous Sediment Gravity Flow Deposits: Practical Criteria for Their Field Description and Classification," Sedimentology **39** (3), 423–454 (1992).
45. J. Guex, *Biochronological Correlations* (Springer-Verlag, Heidelberg–New York–Berlin, 1991).
46. Y. Isozaki, S. Maruyama, and F. Furuoka, "Accreted Oceanic Material in Japan," Tectonophysics **181**, 179–205 (1990).
47. R. Jud, "Biochronology and Systematics of Early Cretaceous Radiolarian of the Western Tethys," Mem. Geol. (Lausanne) **19**, 147 (1994).
48. K. Kiminami, K. Niida, and H. Ando, Cretaceous–Paleogene Arc-Trench System in Hokkaido, Ed. by M. Adachi and K. Suzuki, in *Proceedings of 29th IGC Field Trip Guidebook. Vol. 1 Paleozoic and Mesozoic Terranes: Basement of Japanese Island Arc, Nagoya, Japan, 1992* (Nagoya Univ., 1992), pp. 1–43.
49. G. Kimura, V. S. Rozhdestvensky, K. Okumura, et al., "Mode of Mixture of Oceanic Fragments and Terrigenous Trench Fill in An Accretionary Complex: Example from Southern Sakhalin," Tectonophysics **202** (2–4), 361–374 (1992).
50. G. Kimura and J. Ludden, "Peeling Oceanic Crust in Subduction Zones," Geology **23**, 217–220 (1995).
51. G. Kimura, S. Maruyama, Y. Isozaki, and M. Terabayashi, "Well-Preserved Underplating Structure of the Jadeitized Franciscan Complex, Pacheco Pass, California," Geology **24**, 75–78 (1996).
52. D. R. Lowe, "Sediment Gravity Flows: Their Classification and Some Problems of Application to Flows and Deposits," in *Geology of Continental Slopes*, SEPM Spec. Publ. **27**, 75–82 (1979).
53. S. Maruyama and T. Seno, "Orogeny and Relative Plate Motions—Example of the Japanese Islands," Tectonophysics **127** (3/4), 305–329 (1986).
54. T. Matsuda and Y. Isozaki, "Well-Documented Travel History of Mesozoic Pelagic Chert in Japan: From Remote Ocean to Subduction Zone," Tectonics **10**, 475–499 (1991).
55. A. Matsuoka and A. Yao, "Southern Chichibu Terrane," in *Pre-Cretaceous Terranes of Japan. Publication of IGCP Project, 224*, Ed. by K. Ichikawa, S. Mizutani, I. Hara, S. Hada, and A. Yao (Osaka, 1990), pp. 203–216.
56. B. A. Natal'in, "History and Modes of Mesozoic Accretion in Southeastern Russia, Island Arc" **2** (1), 15–34 (1993).
57. L. Dogherty, "Biochronology and Paleontology of Mid-Cretaceous Radiolarians from Northern Apen-

nines (Italy) and Betic Cordillera (Spain)," Mem. Geol. (Lausanne) **21**, 413 (1994).

58. L. Dogherty and J. Guex, "Rates and Pattern of Evolution Among Cretaceous Radiolarians: Relations with Global Paleoceanographic Events," Micropaleontology **48** (1), 1–22 (2002).
59. J. G. Ogg, G. Ogg, and F. M. Gradstein, *The Concise Geologic Time Scale* (University Press, Cambridge, 2008).
60. D. J. W. Piper, "Turbidite Origin of Some Laminated Mudstones," Geological Magazine **109** (2), 115–126 (1972).
61. J. Savary and J. Guex, "Discrete Biochronological Scales and Unitary Associations: Description of the BioGraph Computer Programm," Mem. Geol. (Lausanne) **34**, 281 (1999).
62. A. M. C. Sengör and B. A. Natal'in, "Turkic-Type Orogeny and Its Role in the Making of the Continental Crust," Annu. Rev. Earth Planet. Sci. **24**, 263–337 (1996).
63. "Shipboard Scientific Party. Synthesis of Shipboard Results: Leg 110 Transect of the Northern Barbados Ridge," in *Proceedings of the Ocean Drilling Program, Initial Reports*, Ed. by A. Mascle, J. C. Moore, et al. (College Station, 1988), Vol. 110, pp. 577–591.
64. "Shipboard Scientific Party. Site 673," in *Proceedings of the Ocean Drilling Program, Initial Reports*, Ed. by A. Mascle, J. C. Moore, et al. (College Station, 1988), Vol. 110, pp. 311–388.
65. "Shipboard Scientific Party. Site 674," in *Proceedings of the Ocean Drilling Program, Initial Reports*, Ed. by A. Mascle, J. C. Moore, et al. (Texas A & M University, College Station, 1988), Vol. 110, pp. 389–485.
66. "Shipboard Scientific Party. Site 808," in *Proceedings of the Ocean Drilling Program, Part A: Initial Reports*, Ed. by A. Taira, I. Hill, J. V. Firth et al., 1991. V. 131. (Texas A & M University, College Station, 1991), Vol. 131, pp. 71–279.
67. "Shipboard Scientific Party. Site 1175," in *Proceedings of the Ocean Drilling Program, Unitial Reports*, Ed. by G. F. Moore, A. Taira, A. Klaus, et al., (College Station, Texas, Ocean Drilling Program, 2001), Vol. 190. http://www-odp.tamu.edu/publications/190_IR/chap_06/chap_06.htm.
68. "Shipboard Scientific Party. Site 1176," in *Proceedings of the Ocean Drilling Program, Initial Reports*, Ed. by G. F. Moore, A. Taira, A. Klaus, et al. (College Station, Texas, Ocean Drilling Program, 2001), Vol. 190. http://www-odp.tamu.edu/publications/190_IR/chap_07/chap_07.htm.
69. "Shipboard Scientific Party. Site 1178," in *Proceedings of the Ocean Drilling Program, Initial Reports*, Ed. by G. F. Moore, A. Taira, A. Klaus, et al. (College Station, Texas, Ocean Drilling Program, 2001), Vol. 190. http://www-odp.tamu.edu/publications/190_IR/chap_09/chap_09.htm.
70. E. A. Silver, M. J. Ellis, N. A. Breen, and T. H. Shipley, "Comments on Growth of Accretionary Wedges," Geology **13**, 6–9 (1985).
71. M. B. Underwood and S. B. Bachman, "Sedimentary Facies Associations within Subduction Complexes," Ed. by J. K. Leggett in *Trench–Forearc Geology*, Geol. Soc. London Spec. Publ. **10**, 537–550 (1982).
72. R. G. Walker, "Deep-Water Sandstone Facies and Ancient Submarine Fans: Model for Exploration for Stratigraphic Traps," AAPG Bull. **62** (6), 932–966 (1978).

Recommended for publishing by G.L. Kirillova